JOURNAL OF PETROLOGY | VOLUME 52 | NUMBER 5 | PAGES 857–890 | 2011 | doi:10.1093/petrology/egr005

Large-volume Rhyolite Genesis in Caldera Complexes of the Snake River Plain: Insights from the Kilgore Tuff of the Heise Volcanic Field, Idaho, with Comparison to Yellowstone and Bruneau–Jarbidge Rhyolites

KATHRYN E. WATTS[1]*, ILYA N. BINDEMAN[1†] AND AXEL K. SCHMITT[2]

[1]DEPARTMENT OF GEOLOGICAL SCIENCES, 1272 UNIVERSITY OF OREGON, EUGENE, OR 97403, USA

[2]DEPARTMENT OF EARTH AND SPACE SCIENCES, UNIVERSITY OF CALIFORNIA, LOS ANGELES, CA 90095, USA

RECEIVED MAY 31, 2010; ACCEPTED JANUARY 25, 2011

Generation of large-volume rhyolites in the shallow crust is an important, yet enigmatic, process in the Snake River Plain and worldwide. Here, we present data for voluminous rhyolites from the 6·6–4·5 Ma Heise volcanic field in eastern Idaho. Heise is arguably the best site to evaluate shallow rhyolite genesis in the Snake River Plain; it is the youngest complete record of caldera cluster volcanism along the Yellowstone hotspot track and it culminated with the eruption of the most voluminous low-$\delta^{18}O$ rhyolite known on Earth: the 1800 km^3 Kilgore Tuff ($\delta^{18}O = 3{\cdot}4‰$). Such low-$\delta^{18}O$ values fingerprint meteoric waters, and thus the shallow crust. New oxygen isotope data for phenocrysts, obtained by laser fluorination, correspond to a low-$\delta^{18}O$ magma value of $3{\cdot}4 \pm 0{\cdot}1‰$ (2 standard error) for Kilgore Tuff samples erupted >100 km apart; however, ion microprobe data for single zircon crystals show significant diversity, with $\delta^{18}O$ values that range from −1·3‰ to 6·1‰. U–Pb zircon ages, mineral chemistry, whole-rock major and trace element geochemistry, Sr and Nd isotope data, and magmatic (liquidus) temperatures are similar and/or overlapping for all studied samples of the Kilgore Tuff. Normal-$\delta^{18}O$ Heise tuff units that preceded the Kilgore Tuff define a temporal compositional trend in trace element concentrations, trace element ratios, and Sr and Nd isotope ratios that is consistent with fractional crystallization from a common reservoir, whereas low-$\delta^{18}O$ Kilgore cycle units have compositions that define a sharp reversal in the temporal trend back towards the composition of the first normal-$\delta^{18}O$ Heise tuff (6·62 Ma Blacktail Creek Tuff). The data support derivation of the voluminous low-$\delta^{18}O$ Kilgore Tuff from remelting of hydrothermally altered (^{18}O depleted) intracaldera and subvolcanic portions of the Blacktail Creek Tuff. Single pockets of melt with variable low-$\delta^{18}O$ values were assembled and homogenized on a caldera-wide scale prior to the climactic Kilgore Tuff eruption, and the best record of this process is provided by the $\delta^{18}O$ diversity in Kilgore Tuff zircons. Temporal trends of oxygen isotopic depletion and recovery in rhyolite eruptions of the Heise volcanic field are clearly linked to caldera collapse events, and remarkably consistent with trends in the Yellowstone Plateau volcanic field. At Heise and Yellowstone, magmatic $\delta^{18}O$ values can be predicted on the basis of cumulative eruptive volumes, with a decrease in $\delta^{18}O$ by ∼1‰ for every ∼1000 km^3 of erupted rhyolite. The Kilgore Tuff of the Heise volcanic field has the same timing, magnitude of $\delta^{18}O$ depletion, and cumulative eruptive volume as the youngest phase of voluminous rhyolitic eruptions in the Yellowstone Plateau volcanic field, indicating that the Kilgore Tuff may serve as a useful analog for these and perhaps other large-volume low-$\delta^{18}O$ rhyolites on Earth.

KEY WORDS: *caldera; Heise; oxygen isotopes; rhyolite; Snake River Plain, zircon*

*Corresponding author. E-mail: kwatts@uoregon.edu
†E-mail: address: bindeman@uoregon.edu

INTRODUCTION

The Snake River Plain–Yellowstone Plateau (SRP–YP) volcanic province in the western USA is one of the largest and most productive silicic igneous provinces on Earth (Fig. 1 inset; Mason *et al.*, 2004). Explosive caldera-forming rhyolite eruptions delineate the 16 Myr track of the Yellowstone hotspot in the SRP (Pierce & Morgan, 1992), with spatially overlapping, or nested, caldera complexes in the two youngest centers (Fig. 1 inset; Christiansen, 2001; Morgan & McIntosh, 2005). In each caldera center, volcanism begins with uplift along the axis of the Yellowstone hotspot swell (Smith & Braile, 1994) and ends with subsidence of the crust and burial by younger basalt flows. SRP rhyolites are typically hot and dry (Branney *et al.*, 2008), and have radiogenic isotope values that require a significant mantle component (Hildreth *et al.*, 1991; Nash *et al.*, 2006; McCurry & Rodgers, 2009).

One of the most striking aspects of rhyolitic volcanism in the SRP–YP province is the extreme abundance of low-$\delta^{18}O$ rhyolite; more than 10 000 km^3 of low-$\delta^{18}O$ ($\delta^{18}O < 6‰$) rhyolites have erupted in the SRP over the past 16 Myr (Hildreth *et al.*, 1984; Bindeman & Valley, 2001; Boroughs *et al.*, 2005; Bindeman *et al.*, 2007). Such magmas require a significant component of oxygen derived from low-$\delta^{18}O$ meteoric waters, and thus fingerprint the shallow (<10 km) crust (Taylor, 1986). Understanding the process by which voluminous low-$\delta^{18}O$ SRP magmas are formed is critical to evaluation of past and present volcanism in the SRP–YP volcanic province. The low-$\delta^{18}O$ SRP rhyolites may also provide important insights into shallow rhyolite genesis worldwide, particularly in regions where meteoric waters are not as strongly depleted in ^{18}O (e.g. equatorial latitudes, low elevations), and consequently do not imprint rhyolites with low-$\delta^{18}O$ signatures that would reveal their shallow crustal origins.

Although some workers advocate melting of a pre-Miocene hydrothermally altered low-$\delta^{18}O$ crustal source, such as the Idaho Batholith (Fig. 1 inset), to explain low-$\delta^{18}O$ rhyolite genesis in the SRP (Boroughs *et al.*, 2005), the normal–high $\delta^{18}O$ signatures of the vast majority of the Idaho Batholith (Criss & Fleck, 1987) and xenoliths of SRP basement rocks (Watts *et al.*, 2010) argue against direct derivation from a pre-existing low-$\delta^{18}O$ crustal source. Influx of meteoric waters and/or assimilation of hydrothermally altered (low-$\delta^{18}O$) wall-rocks into magmas (Hildreth *et al.*, 1984) presents significant mass-balance problems (Taylor, 1986), but wholesale remelting of hydrothermally altered intracaldera blocks eliminates some of these mass-balance constraints (Bindeman *et al.*, 2008).

As the most voluminous low-$\delta^{18}O$ rhyolite in the SRP and worldwide, the Kilgore Tuff is a key unit to evaluate outstanding questions concerning low-$\delta^{18}O$ rhyolite genesis. To investigate the origin of the low-$\delta^{18}O$ Kilgore Tuff, we performed oxygen isotope analyses of phenocrysts from all major caldera-forming tuffs and lavas of the Heise volcanic field. We determined U–Pb zircon ages, which were synthesized with Ar–Ar eruption ages (Morgan & McIntosh, 2005), to determine crystal residence time scales and to assess the connection between zircon age zoning/inheritance and $\delta^{18}O$ depletion in Heise tuffs and lavas, as has been found for Yellowstone rhyolites (Bindeman *et al.*, 2001, 2008). We determined major and trace element geochemistry, mineral chemistry, Sr and Nd isotopic geochemistry, and magmatic temperatures to compare the geochemical identities of normal-$\delta^{18}O$ and low-$\delta^{18}O$ Heise rhyolites and to document temporal compositional variations.

We compare all of the new Heise data presented here with published data for two of the best-studied caldera centers in the SRP that, like Heise, have generated large volumes of low-$\delta^{18}O$ rhyolite: the Yellowstone Plateau volcanic field in the eastern SRP and the Bruneau–Jarbidge volcanic field in the central SRP (Fig. 1 inset). We propose a general model of rhyolite genesis in the SRP that satisfies all the available data for the low-$\delta^{18}O$ Kilgore Tuff cycle, and highlight patterns in caldera cluster evolution that predict its appearance in the Heise volcanic field. Furthermore, this work provides multiple lines of evidence that voluminous crystal-poor silicic magmas can be generated rapidly in the shallow crust by batch assembly of isotopically heterogeneous pockets of melt. This process occurs on time scales that are within error of U-Pb zircon dating methods.

GEOLOGICAL BACKGROUND

The Heise volcanic field is located in eastern Idaho, immediately SW of the younger Yellowstone Plateau volcanic field in western Wyoming (Fig. 1). Like Yellowstone, Heise is a well-preserved volcanic field, with a large (~100 km × 100 km) nested caldera complex and extensive deposits along the margins of the SRP and lower elevations of the surrounding Basin and Range mountains (Fig. 1; Morgan & McIntosh, 2005). Exposures of the Kilgore Tuff span ~20 000 km^2 across parts of Idaho, Montana and Wyoming, and range from <3 m to >120 m thick, with the thickest deposits located near three inferred source vent areas along the northern and southern margin of the Kilgore caldera (Fig. 1; Morgan & McIntosh, 2005). According to anisotropy of magnetic susceptibility (AMS) measurements and grain-size distributions (Morgan, 1988), the three source vents of the Kilgore Tuff are separated by lateral distances of ~50–100 km; two of the vents are located in areas where the Kilgore caldera overlaps the older Heise caldera boundaries (Fig. 1).

The 1800 km^3 Kilgore Tuff is the youngest and most voluminous of four major caldera-forming eruptions in the Heise volcanic field (Table 1; Morgan & McIntosh, 2005).

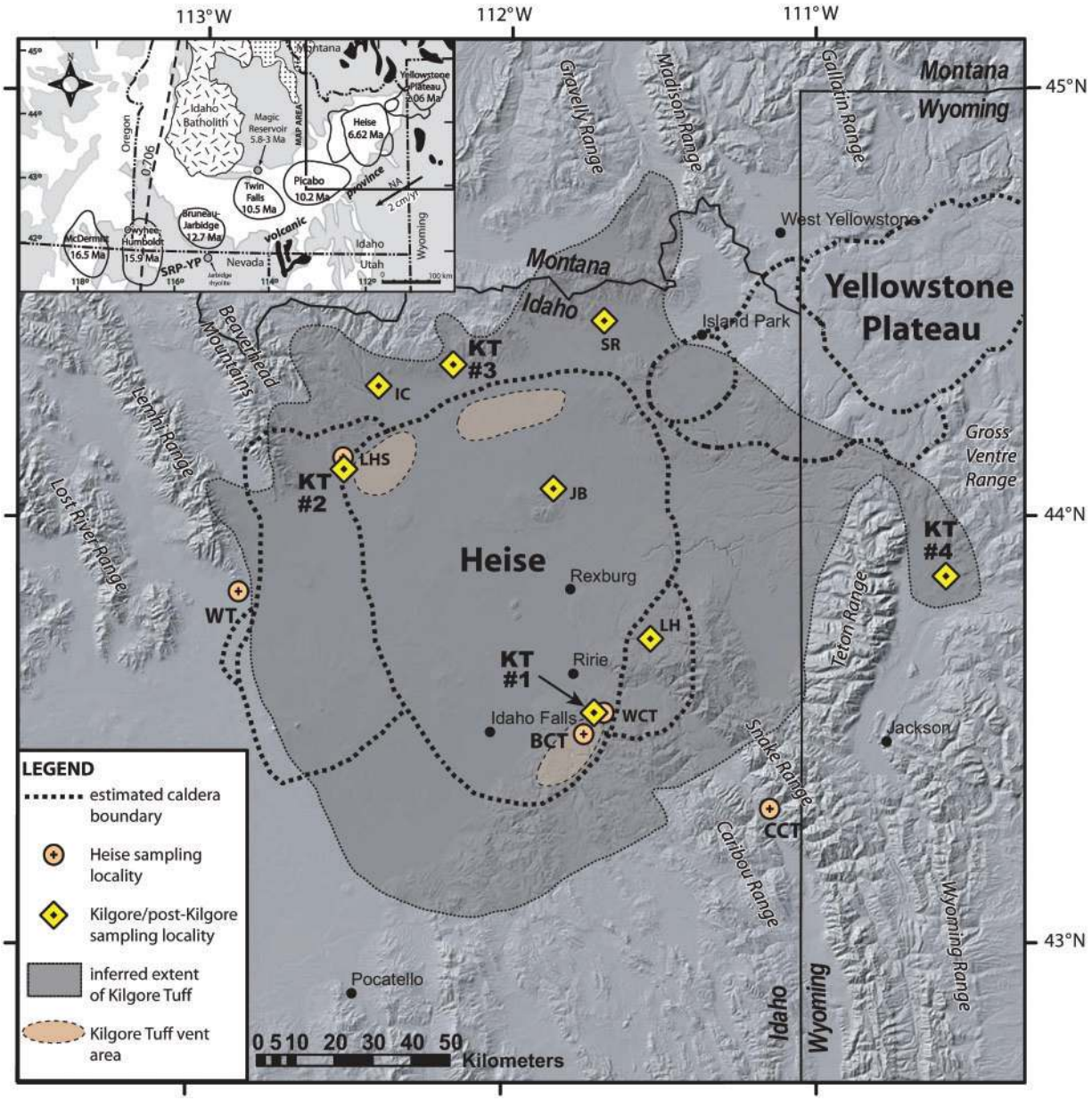

Fig. 1. Map showing the location of the Heise volcanic field in the eastern Snake River Plain (SRP). The Yellowstone Plateau volcanic field, located immediately to the NE, is also indicated. Caldera boundaries at Heise (Morgan & McIntosh, 2005) and Yellowstone Plateau (Christiansen, 2001) are indicated by the bold dashed lines. Sampling localities for the Heise units presented in this study are shown by the symbols, with labels that correspond to the Map ID column in Table 1. Kilgore Tuff sampling localities are indicated in bold (KT #1–4). The inferred extent of the the Kilgore Tuff ignimbrite is shaded in dark gray, and Kilgore Tuff vent areas are bounded by fine dashed lines (taken from Morgan & McIntosh, 2005). Inset in the upper left corner is a generalized map of the Snake River Plain–Yellowstone Plateau (SRP–YP) volcanic province showing the locations and ages of the major volcanic fields and crustal features, including outcrops of Archean (black) and Proterozoic (stippled) basement, and the Jurassic–Eocene Idaho batholith (short-line shading). The $^{87}Sr/^{86}Sr = 0{\cdot}706$ line defines a west to east transition from Mesozoic–Paleozoic accreted oceanic terranes ($^{87}Sr/^{86}Sr < 0{\cdot}706$) to the Precambrian craton of North America ($^{87}Sr/^{86}Sr > 0{\cdot}706$).

The three major caldera-forming eruptions that preceded it include the 1200 km^3 Blacktail Creek Tuff, 750 km^3 Walcott Tuff, and 300 km^3 Conant Creek Tuff (Morgan & McIntosh, 2005). Based on intracaldera and extracaldera areas of 7000 km^2 and 13 000 km^2, respectively (Fig. 1; Morgan & McIntosh, 2005), and an average extracaldera deposit thickness of 50 m (Morgan, 1988; Morgan & McIntosh, 2005), minimum intracaldera and extracaldera

Table 1: Volumes, Ar–Ar ages, U–Pb ages, O, Sr, and Nd isotopic compositions, and temperatures of Heise samples

	Unit	Sample	Map ID	Volume (km^3)	Ar–Ar eruption age (Ma)	U–Pb concordia age (Ma) (*n*)	$\delta^{18}O$ (‰) average			Magma (‰) (Calc.)	Temperature (°C)			$^{87}Sr/^{86}Sr_i$	$^{143}Nd/^{144}Nd$
							Quartz	Zircon	Sanidine		Ti-in-zrc	Zrc sat	Liq		
I	Blacktail Creek Tuff	95-2001a	BCT	1200	6·62 ± 0·03	6·92 ± 0·28 (12)	6·40	4·81	—	6·6	819	848	869	0·71238	0·51214
II	Walcott Tuff	06HS-18	WT	750	6·27 ± 0·04	6·37 ± 0·26 (10)	—	4·17	5·57	6·1	—	786	861	0·70991	0·51216
	Lidy Hot Springs rhyolite	08HS-10	LHS	>10?	6·20 ± 0·05	—	—	—	3·68	4·4	—	822	871	0·71137	0·51214
	Kelly Canyon rhyolite	1103·1	—	>10?	5·7 ± 0·1*	—	—	—	5·66	6·4	—	—	—	—	—
	Wolverine Creek Tuff	06HS-16	WCT	<100?	5·59 ± 0·05	5·45 ± 0·14 (15)	—	—	5·83	6·5	—	799	868	0·70947	0·51233
III	Conant Creek Tuff	06HS-5	CCT	300	5·51 ± 0·13	5·70 ± 0·19 (10)	—	3·96	5·52	5·9	*709*	859	949	0·70894	0·51229
	Pre-Kilgore Tuff	06HS-14	KT #1	?	—	4·87 ± 0·20 (10)	3·29	1·89	2·81	3·5	—	945	990	0·71071	0·51214
IV	Kilgore Tuff	TNP96-43	KT #4	1800	4·52 ± 0·07	4·49 ± 0·25 (12)	4·33	1·61	2·88	3·4	808	874	871	0·71028	0·51222
	Kilgore Tuff	95-2017b	KT #2	1800	4·51 ± 0·05	4·59 ± 0·26 (10)	4·29	1·50	2·74	3·3	826	842	872	0·71037	0·51224
	Kilgore Tuff	95-2015	KT #3	1800	4·44 ± 0·07	—	—	—	2·93	3·6	—	852	871	—	—
	Kilgore Tuff	06HS-10	KT #1	1800	4·43 ± 0·08	4·58 ± 0·24 (10)	—	—	2·65	3·3	—	850	870	0·71047	0·51221
	Kilgore Tuff	06HS-11	KT #1	1800	4·43 ± 0·08	4·58 ± 0·18 (10)	—	—	2·97	3·6	—	842	870	0·71065	0·51222
	Kilgore Tuff	95-2010	KT #1	1800	4·43 ± 0·08	—	—	—	2·71	3·3	—	849	872	—	—
	Juniper Buttes rhyolite	06HS-4A	JB	>10?	—	4·29 ± 0·15 (9)	—	—	3·86	3·7	*730*	811	871	0·70985	0·51219
	Long Hollow rhyolite	626·1	LH	>10?	—	4·28 ± 0·18 (13)	4·51	1·83	3·88	3·7	—	816	871	0·70917	0·51219
	Indian Creek rhyolite	06HS-1	IC	>10?	—	3·96 ± 0·18† (6) 4·11 ± 0·27‡ (6) 4·46 ± 0·17§ (21)	—	1·23	3·44	3·0	*782*	858	875	0·71073	0·51223
	Sheridan Reservoir rhyolite¶	06HS-19	SR	>10?	—	2·07 ± 0·19 (14)	4·53	2·34	3·79	4·0	*784*	886	864	0·71815	0·51199

Roman numerals signify the four major caldera-forming cycles of the Heise volcanic field. Volumes are from Morgan & McIntosh (2005), and estimated for units without published volumes. $^{40}Ar/^{39}Ar$ eruption ages with 2σ are from Morgan & McIntosh (2005) for the same Heise units or samples or sampling localities. $^{206}Pb/^{238}U$ concordia ages with 95% confidence intervals are from this study and Bindeman *et al.* (2007); TNP96-43 and 95-2017b ages are corrected for a typesetting error in Table 1 of Bindeman *et al.* (2007). Magma $\delta^{18}O$ values were calculated from phenocryst analyses, with fractionation factors from Bindeman & Valley (2002) for zircon ($\Delta^{18}O_{melt\text{-}zircon} = 1{\cdot}6\text{–}1{\cdot}9$‰) and Bindeman *et al.* (2001) for sanidine ($\Delta^{18}O_{melt\text{-}sanidine} = 0{\cdot}5\text{–}0{\cdot}7$‰) for liquidus temperatures of 800–950°C. (See Supplementary Data Table 3 for compilation of all Heise $\delta^{18}O$ data.) TiO_2 activity for Ti-in-zircon temperatures was calculated modifying a procedure in Wark *et al.* (2007) using published ilmenite and ulvöspinel compositions and temperatures for Heise units (Henshaw, 2002); $aTiO_2$ ranged from 0·39 to 0·50. Ti-in-zircon temperatures in italics were calculated using the average $aTiO_2$ for Heise rhyolites (0·5). Zircon saturation temperatures were calculated from whole-rock compositions as done by Watson & Harrison (1983). Liquidus temperatures were calculated with MELTS at 1·5 kbar and 3 wt % H_2O.

*Old K–Ar age published by Morgan & McIntosh (2005).

†Rims (0–2 μm).

‡Rims (5–7 μm).

§Cores.

¶Post-Huckleberry Ridge Tuff unit (see text for details).

volumes of 350 km^3 and 650 km^3, *c.* 1000 km^3 total volume, are conservative volume estimates for the Kilgore Tuff. The intracaldera thickness of the Kilgore Tuff is not known, but if comparable with the 1 km thickness observed for other large-volume tuffs (e.g. Bishop Tuff), then a much larger total volume of *c.* 8000 km^3 is possible. An approximation of intracaldera volume as twice the extracaldera volume (Bacon, 1983) yields an intracaldera volume of 1300 km^3, *c.* 2000 km^3 total volume, which is similar to the 1800 km^3 volume estimate published by Morgan & McIntosh (2005). As most Heise tuff exposures are densely welded ignimbrite (see Branney *et al.*, 2008), the dense rock equivalent (DRE) volumes are in effect equal to the rock volumes.

Like voluminous caldera-forming tuffs at Yellowstone, the Kilgore Tuff and other Heise tuffs erupted through Archean crust, a fact confirmed by the location of the Heise volcanic field ~300 km east of the 0·706 isopleth that defines the west–east transition from Mesozoic accreted terranes ($^{87}Sr/^{86}Sr < 0{\cdot}706$) to the Precambrian craton of North America ($^{87}Sr/^{86}Sr > 0{\cdot}706$), Archean crustal xenolith localities that extend from 111·7°W to 114·5°W along the axis of the SRP (Leeman *et al.*, 1985; Watts *et al.*, 2010), and exposures of Archean basement rocks that surround the eastern SRP (Fig. 1 inset). The Cretaceous–Eocene Idaho Batholith forms significant surface outcrops in the central SRP (Fig. 1 inset), but its eastern boundary is ~200 km west of the Heise volcanic field, and thus it is not likely to be a crustal source of the Kilgore Tuff or any of the other eastern SRP tuffs (see Boroughs *et al.*, 2005).

Smaller volume post-Kilgore rhyolites erupted effusively near the inferred ring fracture zone and as resurgent domes within the Kilgore caldera (Fig. 1; Morgan & McIntosh, 2005). The Indian Creek rhyolite and Long Hollow rhyolite are located ~10 km north and ~5 km east of the Kilgore caldera boundary, respectively (Fig. 1). The Juniper Buttes rhyolite is located in the center of the Kilgore caldera (Fig. 1), and occurs as a glassy dome complex with a well-defined rectilinear fault pattern that is comparable in scale with resurgent domes in large caldera complexes elsewhere (Morgan & McIntosh, 2005). The central location of the Juniper Buttes dome complex relative to the inferred Kilgore Tuff source vents (Fig. 1), and the presence of Kilgore Tuff exposures within the dome complex, support the interpretation that it is a young resurgent dome of the Kilgore caldera (Morgan & McIntosh, 2005).

METHODS

U–Pb dating of Heise zircons was performed with a CAMECA ims 1270 ion microprobe at The University of California, Los Angeles (UCLA). Approximately 20–30 zircon grains from each sample were hand-picked, mounted in epoxy, polished to ~75% of their original size, and mapped using reflected light and back-scatter electron microscopy. We followed standard protocols for the analysis of youthful zircons (Schmitt *et al.*, 2003; Bindeman *et al.*, 2006). Ion intensities were measured in 12–15 cycles using a mass-filtered ^{16}O-primary ion beam of ~15 nA focused to an oval 25–30 μm spot. AS3 (Paces & Miller, 1993) reference zircons were used to calibrate U, Th, and Pb sensitivities. U–Pb ages were adjusted for initial U–Th disequilibrium using techniques described by Schärer (1984), Reid (2003), and Bindeman *et al.* (2006), typically resulting in an ~80 kyr age increase.

Oxygen isotope analyses were performed at the University of Oregon stable isotope laboratory using CO_2-laser fluorination (e.g. Bindeman, 2008). Single and bulk silicate mineral grains, ranging in weight between 0·6 and 2 mg, were reacted in the presence of BrF_5 reagent to liberate oxygen gas. The gas generated in the laser chamber was purified through a series of cryogenic traps held at liquid nitrogen temperature, and a mercury diffusion pump was used to remove traces of fluorine gas. Oxygen was converted to CO_2 gas in a small platinum–graphite converter, the yield was measured, and then CO_2 gas was analyzed on a MAT 253 mass spectrometer. Four to seven Gore Mt. Garnet ($\delta^{18}O = 5{\cdot}75‰$) standards were analyzed together with the unknowns during each analytical session. Variability of the measured $\delta^{18}O$ values of the standards ranged from 0·1 to 0·25‰ less than their empirical value, and unknown samples were adjusted to correct for this small day-to-day variability on the SMOW scale. The average precision on standards and duplicates of single grains and bulk analyses was better than 0·1‰. A small subset of zircons were analyzed for oxygen isotopes with a CAMECA ims 1270 ion microprobe at UCLA. For these analyses, we targeted the same zircon spots (after repolishing) as dated by U–Pb, following the polishing protocols of Kita *et al.* (2009) to ensure maximum flatness of the mount. Instrumental calibrations and analytical methods were the same as those used for the Bindeman *et al.* (2008) ion microprobe study of Yellowstone zircons.

Major element compositions of plagioclase, orthopyroxene and clinopyroxene phenocrysts were measured with a CAMECA SX-100 electron microprobe at the University of Oregon using a 15 kV accelerating voltage, 30 nA beam current, and a beam diameter of 5 μm. A combination of mineral standards was used. Major and trace element whole-rock X-ray fluorescence (XRF) analyses were obtained at the GeoAnalytical Lab at Washington State University on a ThermoARL Advant'XP+sequential X-ray fluorescence spectrometer. Sr and Nd isotope analyses of crushed whole-rock powders were obtained by isotope dilution-thermal ionization mass spectrometry (ID-TIMS) at Central Washington University.

Magmatic temperatures were calculated using a variety of methods. Ti-in-zircon temperatures were calculated

from Ti concentrations in single zircon phenocrysts using established protocols (Watson & Harrison, 2005). Ti concentrations were measured with a CAMECA ims 1270 ion microprobe at UCLA. Zircon saturation temperatures were calculated using whole-rock major element compositions and the methods of Watson & Harrison (1983). Liquidus temperatures were calculated with whole-rock major element compositions and MELTS thermodynamic modeling software (Ghiorso & Sack, 1995). The MELTS runs were performed at 1·5 kbar and 3 wt % H_2O, which are typical pressures and water contents for eastern SRP rhyolites (Gansecki, 1998).

U–PB ZIRCON GEOCHRONOLOGY

New U–Pb zircon ages for the major tuffs and lavas of the Heise volcanic field were combined with U–Pb zircon ages previously reported by us (Bindeman *et al.*, 2007) and Ar–Ar eruption ages published by Morgan & McIntosh (2005). In total, U–Pb zircon ages have been determined for 13 Heise samples: four samples of the Kilgore Tuff, four samples of post-Kilgore lavas, and five samples of major tuffs that predate the Kilgore Tuff (Table 1). Where direct comparison with $^{40}Ar/^{39}Ar$ eruption ages is possible, disequilibria corrected $^{206}Pb/^{238}U$ zircon crystallization ages overlap within 95% confidence of the eruption ages, and in most cases zircon crystallization ages are ~0·1–0·3 Myr older than the eruption ages, as observed for silicic magma centers worldwide (Table 1; Reid, 2003; Simon *et al.*, 2009). U–Pb zircon crystallization ages of the three major caldera-forming eruptions that preceded the final low-$\delta^{18}O$ Kilgore Tuff cycle, including the normal-$\delta^{18}O$ Blacktail Creek Tuff (6·92 ± 0·28 Ma), Walcott Tuff (6·37 ± 0·26 Ma) and Conant Creek Tuff (5·70 ± 0·19 Ma), are separated by ~500–700 kyr intervals, a periodicity that is similar to the ~750 kyr periodicity of major caldera-forming eruptions at Yellowstone (Lanphere *et al.*, 2002), but is longer than the ~200–400 kyr periodicity of the Bruneau–Jarbidge eruptive center to the west (Fig. 1 inset; Bonnichsen *et al.*, 2008).

In this study we define a new unit that postdates the Conant Creek Tuff and predates the Kilgore Tuff, called here the 'Pre-Kilgore Tuff'. This unit is an airfall deposit collected at the base of a Kilgore Tuff stratigraphic sequence (KT #1 in Fig. 1; see 'Kilgore Tuff stratigraphic sequence' section). It has a U–Pb zircon age of 4·87 ± 0·20 Ma, which is ~300 kyr older than the Kilgore Tuff (Table 1). Although the Pre-Kilgore Tuff is stratigraphically separated from the overlying Kilgore Tuff by ~11 m of paleosols (see 'Kilgore Tuff stratigraphic sequence' section), it has a distinctive, low-$\delta^{18}O$ isotopic signature that is identical to that of the Kilgore Tuff (Table 1). Thus, we classify it as an early eruptive phase of the low-$\delta^{18}O$ Kilgore cycle.

U–Pb zircon crystallization ages of four Kilgore Tuff samples from three localities that span >150 km across eastern Idaho and western Wyoming (KT #1, KT #2, KT #4; Fig. 1) cluster tightly in age, averaging 4·56 ± 0·23 Ma [95% confidence interval (CI)] (Table 1). We found no evidence of significantly older zircons in the low-$\delta^{18}O$ Kilgore Tuff, in contrast to what has been found for low-$\delta^{18}O$ Yellowstone rhyolites (see Bindeman *et al.*, 2001). The difference in the U–Pb zircon crystallization age and Ar–Ar eruption age of the Kilgore Tuff indicates a crystal residence time of ~110 kyr (e.g. Reid, 2003), which is longer than crystal residence timescales of major caldera-forming tuffs at Yellowstone (~15–70 kyr; Bindeman *et al.*, 2001) and shorter than crystal residence timescales of major tuffs at Bruneau–Jarbidge (~300–900 kyr; Cathey & Nash, 2004), but comparable with the ~100–150 kyr crystal residence timescales of many large-volume (>100 km^3) tuffs around the world (e.g. Vazquez & Reid, 2004; Charlier *et al.*, 2005; Simon & Reid, 2005).

Smaller volume post-Kilgore lavas have younger U–Pb ages between 3·96 and 4·29 Ma (Table 1). These units have low-$\delta^{18}O$ signatures that are distinctive of the Kilgore cycle (~3–4‰) and have similar mineral chemistry and major, trace and isotopic geochemistry to the Kilgore Tuff (See 'Oxygen isotopes', 'Petrography and mineral chemistry', and 'Whole-rock geochemistry' sections; Tables 1–3). Their appearance suggests that low-$\delta^{18}O$ magmatism lingered in the Heise volcanic field for ~0·5 Myr after the Kilgore Tuff eruption, periodically tapping residual Kilgore magma beneath the Kilgore caldera. This notion is supported by significant U–Pb age zoning in zircons of the post-Kilgore Indian Creek rhyolite, which have cores (4·46 ± 0·17 Ma) that correspond in age to the Kilgore Tuff, and rims that are ~0·5 Myr younger (Table 1; Bindeman *et al.*, 2007).

The U–Pb age of the Sheridan Reservoir rhyolite (2·07 ± 0·19 Ma) is ~2 Myr younger than any Heise unit, and overlaps in eruption age with the Huckleberry Ridge Tuff [2·06 Ma (Ar–Ar; Lanphere *et al.*, 2002)] and post-Huckleberry Ridge Tuff units [1·86–1·78 Ma (K–Ar; Obradovich, 1992)] of the Yellowstone Plateau volcanic field. Contrary to the previous interpretation that the Sheridan Reservoir rhyolite is a late-stage post-Kilgore unit of the Heise volcanic field (Morgan & McIntosh, 2005; Bindeman *et al.*, 2007), new Sr and Nd isotope data (see 'Strontium and neodymium isotopes section') and trace element data (e.g. Ba concentrations; Table 3), combined with the young U–Pb age and low-$\delta^{18}O$ signature of the Sheridan Reservoir rhyolite (Table 1), suggest that it is a post-Huckleberry Ridge Tuff unit that belongs to the Yellowstone Plateau volcanic field. Temporally and spatially, the Sheridan Reservoir rhyolite is related to the 2·06 Ma Huckleberry Ridge Tuff caldera collapse, and if emanating from the ring fracture of the Huckleberry Ridge Tuff caldera, the lateral distance covered by the

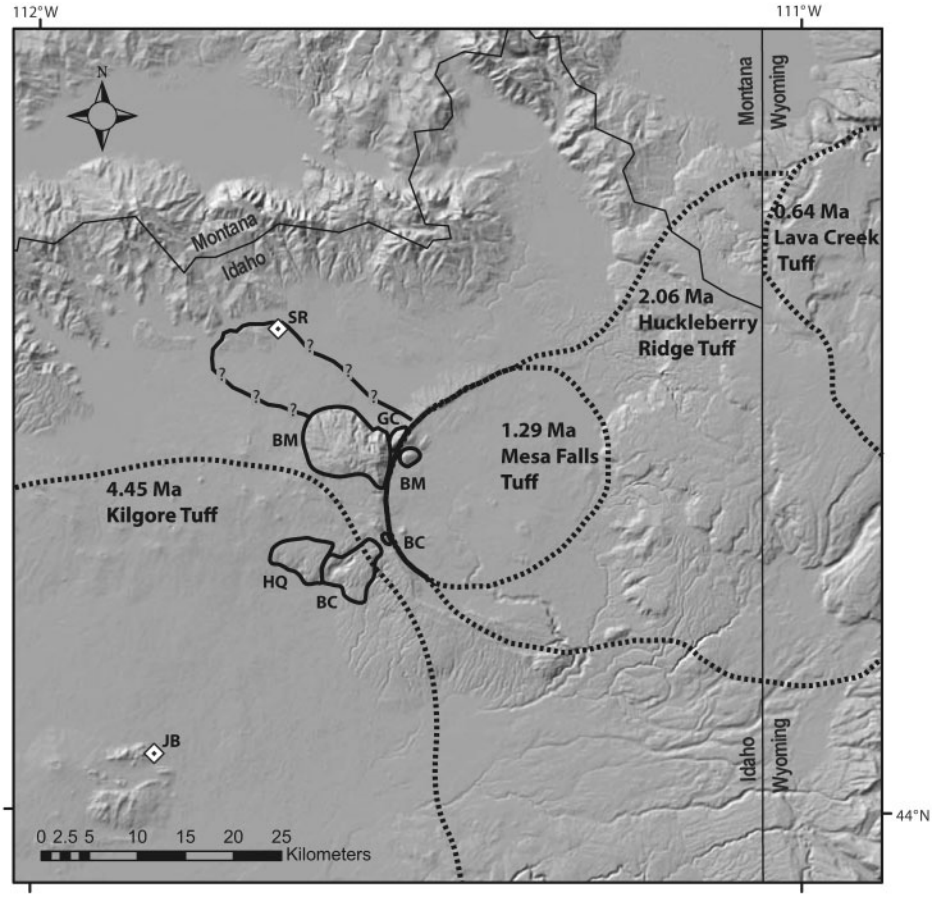

Fig. 2. Detailed location map for the NE part of Fig. 1 showing the locations and ages of the Yellowstone and Heise calderas and the boundaries of post-Huckleberry Ridge Tuff (Yellowstone) rhyolite flows (GC, Green Canyon flow; BM, Bishop Mountain flow; BC, Blue Creek flow; HQ, Headquarters flow). The Sheridan Reservoir rhyolite (SR) is located ~20 km NW of the western margin of the Huckleberry Ridge Tuff caldera and has a U–Pb age (2·07 Ma; Table 1) that is identical to the age of the Huckleberry Ridge Tuff (2·06 Ma; Lanphere *et al.*, 2002). New data for the SR rhyolite presented in this study indicate that it is a post-Huckleberry Ridge Tuff unit, rather than a post-Kilgore Tuff unit (see text for further details).

Sheridan Reservoir rhyolite is ~20 km (Fig. 2). This means that rhyolites comparable in scale with voluminous post-Lava Creek Tuff Central Plateau Member rhyolites may have been produced much earlier in the evolution of the Yellowstone Plateau volcanic field than previously thought (see Christiansen, 2001).

KILGORE TUFF STRATIGRAPHIC SEQUENCE

We investigated in detail one of the type-localities of the Heise volcanic field (KT #1 in Fig. 1), a thick (>14 m) stratigraphic sequence of Heise volcanic rocks and intercalated sediments exposed in a road-cut on Meadow Creek Road in eastern Idaho (Hackett & Morgan, 1988; Morgan & McIntosh, 2005). This stratigraphic section is underlain by the 5·59 Ma Wolverine Creek Tuff of the Heise volcanic field and overlain by the 2·06 Ma Huckleberry Ridge Tuff of the Yellowstone Plateau volcanic field (Fig. 3; Hackett & Morgan, 1988). Thick outflow (8–11 m) and intracaldera (>150 m) facies of the oldest exposed Heise tuff, the Blacktail Creek Tuff, are located along the margins of Ririe Lake, ~5 km west of and stratigraphically below the Meadow Creek road-cut (Hackett & Morgan, 1988).

Although this section has previously been classified as a thick outflow facies ignimbrite of the Kilgore Tuff that was emplaced as several pyroclastic flows in rapid succession (Hackett & Morgan, 1988; Morgan & McIntosh, 2005), our work indicates that only an airfall deposit at the base (08HS-KG-3 and 06HS-14) and a thick (~2 m) vitrophyre at the top (06HS-10, 06HS-11) are primary (Fig. 3). Paleosol structures, coarse lithic layers, and reworked and trough cross-bedded pumice clasts are present throughout the section, providing clear evidence for time breaks between the airfall at the base and the capping vitrophyre (Fig. 3). Whole-rock major and trace element

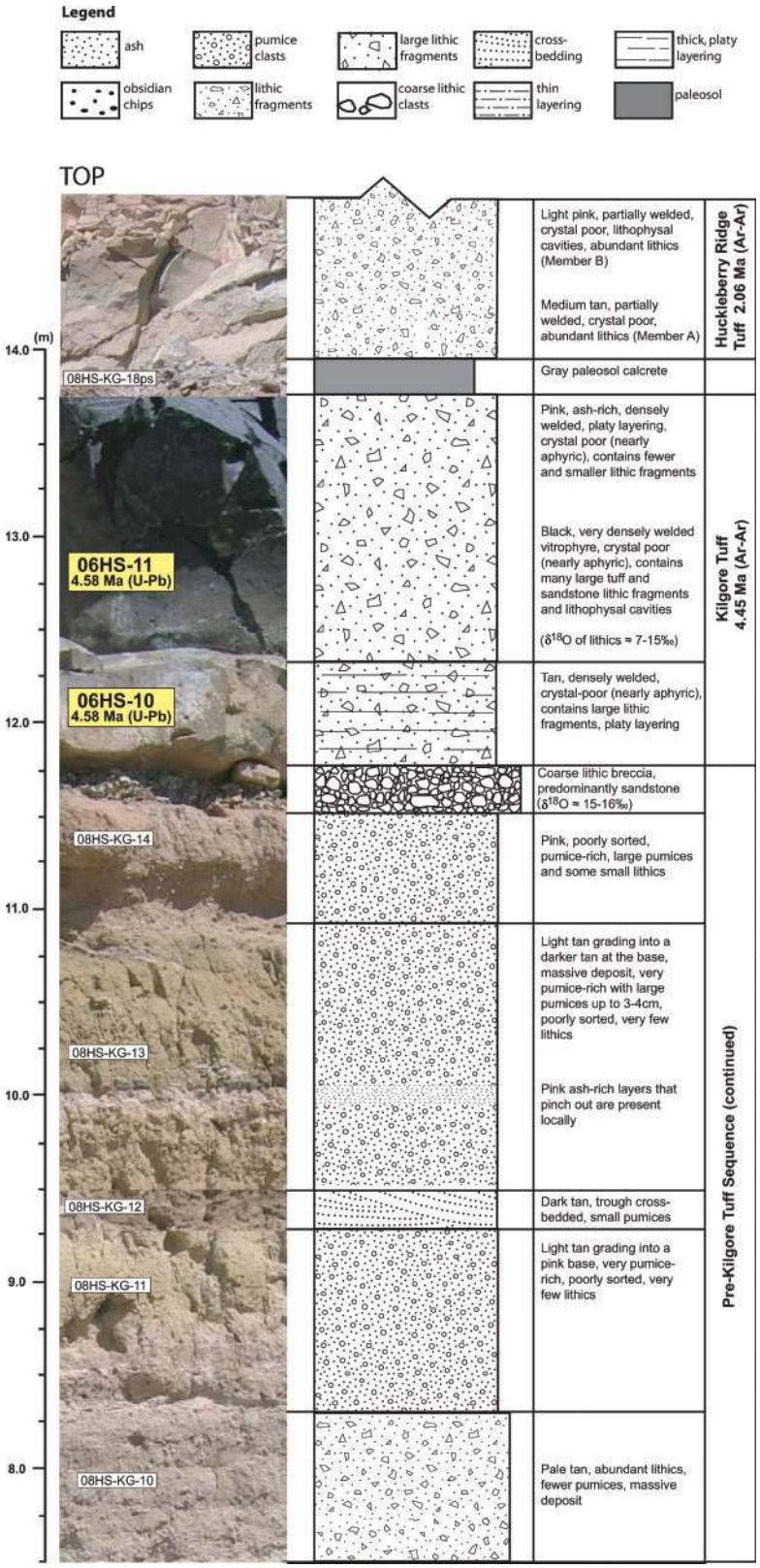

Fig. 3. Stratigraphy of the Heise pyroclastic sequence at Meadow Creek Road in eastern Idaho (site location KT #1 in Fig. 1). Field photographs and descriptions are shown with a schematic stratigraphic section. U–Pb dated units (this study) at the base (Pre-Kilgore Tuff airfall; 4·87 ± 0·20 Ma) and top (Kilgore Tuff vitrophyre; 4·58 ± 0·18 Ma) bracket the age of the pyroclastic rocks and intercalated sediments that form the Pre-Kilgore Tuff sequence. Coarse lithic layers, paleosols, and trough cross beds indicate intervening time breaks. The Pre-Kilgore Tuff airfall is underlain by the Heise Wolverine Creek Tuff (Ar–Ar age of 5·59 ± 0·05 Ma; Morgan & McIntosh, 2005), and the Kilgore Tuff vitrophyre is overlain by the Yellowstone Huckleberry Ridge Tuff (Ar–Ar age of 2·06 ± 0·01 Ma; Lanphere *et al.*, 2002).

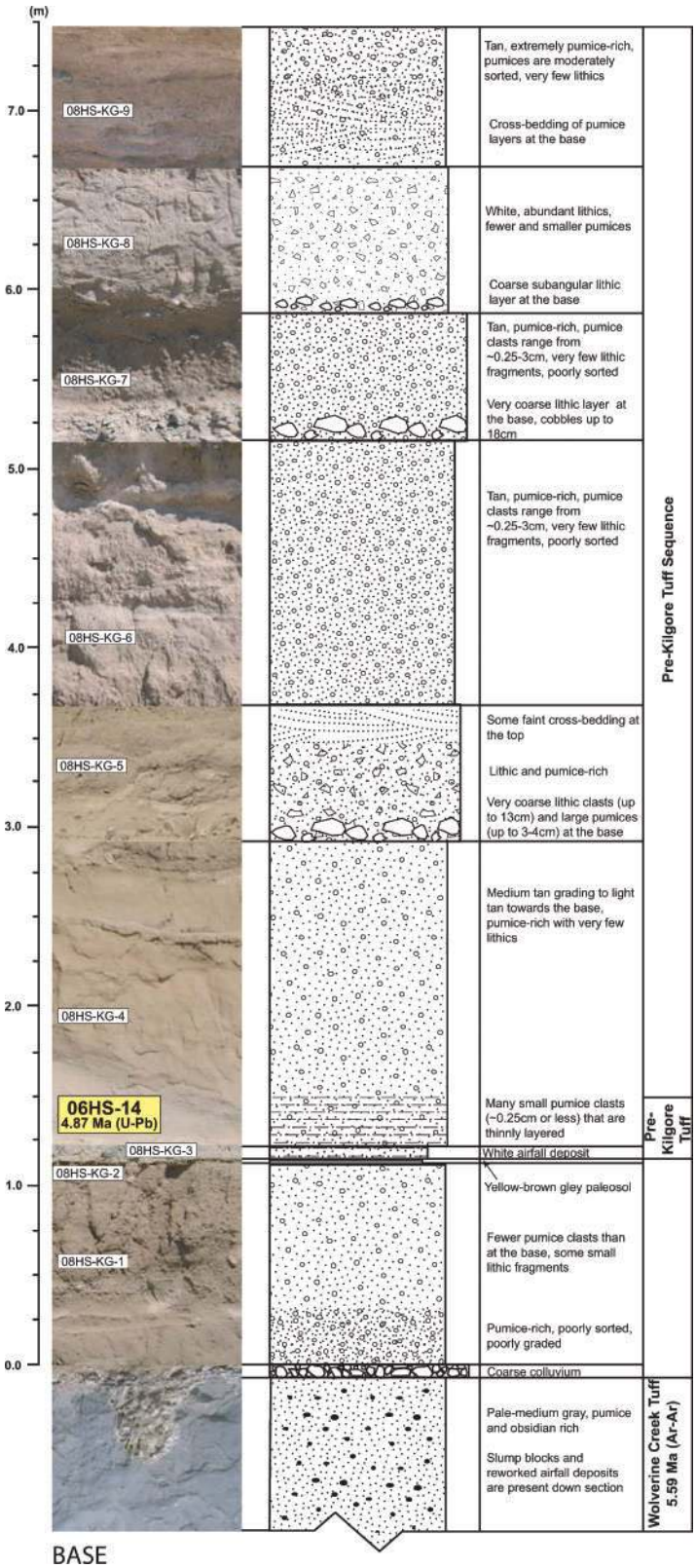

Fig. 3. Continued

geochemistry of 14 samples from this stratigraphic section shows that most samples (excluding the Kilgore Tuff vitrophyre at the top) are moderately to severely altered relative to primary Heise rhyolite compositions, as indicated by lower Na_2O and K_2O, higher FeO, MgO and TiO_2, lower Rb, Ce, Nb and higher Sr (Supplementary Data Table 1, available at http://www.petrology.oxfordjournals.org). In some samples, pumice clasts are cemented by lacustrine calcite. We note that deviations from typical Heise rhyolite compositions are smallest for pumice-rich units of the stratigraphic section, and that nearly all units have trace element concentrations of Ba, Y and Zr that fall within a typical Heise range (Supplementary Data Table 1).

In addition to major and trace element geochemistry, U–Pb zircon ages, oxygen isotope data ($\delta^{18}O$ and $\Delta^{17}O$), and Sr and Nd isotope data were obtained for a subset of samples from this stratigraphic section (Table 1; Fig. 3). U–Pb zircon ages of an airfall at the base, referred to here as the Pre-Kilgore Tuff ($4{\cdot}87 \pm 0{\cdot}20$ Ma), and two samples of a Kilgore Tuff vitrophyre at the top of the section ($4{\cdot}58 \pm 0{\cdot}24$ Ma, $4{\cdot}58 \pm 0{\cdot}18$ Ma), corroborate inferential evidence of paleosol thicknesses and pedotypes (e.g. Retallack *et al.*, 2002; Davis & Ellis, 2010) that the Pre-Kilgore Tuff is tens to hundreds of thousands of years older than the Kilgore Tuff vitrophyre. Although the U–Pb zircon ages of the Pre-Kilgore Tuff and Kilgore Tuff overlap within uncertainty (95% CI), the presence of more than 11 m of intervening sediments requires a significant (at least tens of thousands of years) time break between them. We refer to this sequence of intercalated volcanic rocks and sediments as the Pre-Kilgore Tuff sequence (Fig. 3).

In addition, we determined that a grey paleosol at the base of the section (08HS-KG-2), a trough-cross bedded unit in the middle of the section (08HS-KG-12), and a paleosol calcrete at the top of the section (08HS-KG-18ps) have mass-independent $\Delta^{17}O$ signatures of $+0{\cdot}6$‰, $+1{\cdot}4$‰, and $+0{\cdot}7$‰, respectively, indicating atmospheric oxidation of volcanic SO_2 by ozone during plinian supereruptions (e.g. Martin & Bindeman, 2009). Carbonate nodules in samples 08HS-KG-12 and 08HS-KG-18ps have $\delta^{18}O$ values of 15·27‰ and 16·06‰, and $\delta^{13}C$ values of $-6{\cdot}26$‰ and $-5{\cdot}66$‰, respectively. Using the calcite-H_2O $\delta^{18}O$ paleothermometer of O'Neil *et al.* (1969) and modern meteoric water $\delta^{18}O$ values for eastern Idaho (i.e. -14‰; Bowen *et al.*, 2007), we calculate pedogenic carbonate formation temperatures (i.e. ambient air temperatures) of 20°C (08HS-KG-12) and 17°C (08HS-KG-18ps). Temperature estimates made with calcite-H_2O paleothermometers are prone to large uncertainties due to the uncertainty of the oxygen isotopic composition of the waters from which the calcites precipitated. For instance, a 1‰ change in the $\delta^{18}O$ composition of the water (e.g. owing to evaporation) would change our carbonate formation temperature estimates by ±5°C. Nonetheless, the carbonate formation temperature that we calculate for the paleosol sample overlying the Kilgore Tuff (08HS-KG-18ps) is 3°C cooler than that of the paleosol sample beneath it (08HS-KG-12), and if not due to a pre-existing (i.e. pre-Kilgore) climatic trend, the Kilgore Tuff supereruption may have caused climate cooling by several degrees (e.g. Rampino & Self, 1992).

PETROGRAPHY AND MINERAL CHEMISTRY

Textural and petrographic description of Heise rhyolites

Large-volume tuffs of the Heise volcanic field are crystal poor (1–20 vol. % phenocrysts) with fine-grained groundmass textures that range from loosely welded (pumiceous, undeformed glass shards) to very densely welded (extensive deformation of glass shards, recrystallization of groundmass). Smaller volume lavas are generally more crystal rich than large-volume tuffs, but range from aphyric to porphyritic (Table 2). All Heise rhyolites have a similar mineralogy, yet differ markedly in the percentage of phenocrysts and the presence or absence of quartz (Table 2). Unlike Yellowstone rhyolites, but similar to Bruneau–Jarbidge rhyolites, quartz in Heise rhyolites is typically subordinate to plagioclase and alkali feldspar and smaller in size (<1 mm).

Plagioclase occurs as large (1–3 mm) laths with oligoclase compositions that are similar among all studied Heise units (Table 2; Appendix A; Supplementary Data Table 2). In the normal-$\delta^{18}O$ Blacktail Creek, Walcott and Conant Creek tuff units, plagioclase crystals are mostly anhedral and possess oscillatory core–rim zoning, but in low-$\delta^{18}O$ units of the Kilgore Tuff and post-Kilgore rhyolites, plagioclase is more variable, ranging from anhedral to subhedral and unzoned to zoned, with the more crystal-rich samples (5–20 vol. %) exhibiting the most heterogeneity (e.g. sieved cores, resorbed rims, anhedral cores with overgrowth rims, multiple twin generations; Fig. 4a and b).

Orthopyroxene phenocrysts are unzoned and their compositions cluster tightly for each Heise unit (Table 2; Appendix A; Supplementary Data Table 2). A similar pattern is observed for clinopyroxene compositions, but with more overlap between units (Table 2; Appendix A; Supplementary Data Table 2). The lack of zoning in pyroxene phenocrysts is probably explained by rapid diffusive Fe–Mg re-equilibration with the host melt, as is often observed in high-temperature volcanic rocks (e.g. Cathey & Nash, 2004, 2009; Hildreth & Wilson, 2007), whereas slower diffusion in plagioclase phenocrysts preserves more zoning. Reverse zoning, which would be an indication of reheating, is not observed. We note that distinct pyroxene

Table 2: Petrological summary of Heise samples

Unit	Sample	Phenocrysts		Average phenocryst composition		
		vol. %	Abundance	Plag	Cpx	Opx
Blacktail Creek Tuff	95-2001a*	20	P, Q, A, C, O, F	$Ab_{67}An_{25}Or_9$	$En_{40}Fs_{20}Wo_{41}$	$En_{46}Fs_{51}Wo_3$
Walcott Tuff	06HS-18*	1–2	P, A, Q, C, O, F	$Ab_{69}An_{21}Or_9$	$En_{37}Fs_{22}Wo_{44}$	$En_{51}Fs_{46}Wo_3$
Lidy Hot Springs rhyolite	08HS-10	20	P, A, Q, C, O, F	—	—	—
Wolverine Creek Tuff	06HS-16*	1–2	P, A, C, O, F	$Ab_{71}An_{20}Or_9$	$En_{47}Fs_{14}Wo_{39}$	$En_{34}Fs_{63}Wo_3$
Conant Creek Tuff	06HS-5	5–7	P, A, C, O, F	—	—	—
Pre-Kilgore Tuff	06HS-14	5	P, A, Q, C, O, F	—	—	—
Kilgore Tuff	95-2017b	10	P, A, Q, C, O, F	—	—	—
Kilgore Tuff	TNP 96-43	1–2	P, A, Q, C, O, F	—	—	—
Kilgore Tuff	06HS-10	1–2	P, A, Q, C, O, F	$Ab_{66}An_{26}Or_8$	—	$En_{38}Fs_{58}Wo_4$
Kilgore Tuff	06HS-11	1–2	P, A, Q, C, O, F	$Ab_{69}An_{24}Or_8$	$En_{28}Fs_{32}Wo_{40}$	—
Juniper Buttes rhyolite	06HS-4a	1–2	P, A, C, O, F	$Ab_{64}An_{30}Or_6$	$En_{37}Fs_{20}Wo_{43}$	$En_{56}Fs_{41}Wo_3$
Long Hollow rhyolite	626.1	20	P, Q, A, O, C, F	—	—	—
Indian Creek rhyolite	06HS-1	5	P, A, C, O, F	$Ab_{70}An_{20}Or_{10}$	$En_{30}Fs_{30}Wo_{40}$	$En_{37}Fs_{60}Wo_4$
Sheridan Reservoir rhyolite	06HS-19	10	P, Q, A, C, O, F	—	—	—

P, plagioclase; Q, quartz; A, alkali feldspar; O, orthopyroxene; C, clinopyroxene; F, Fe–Ti oxides. Trace amounts of apatite and zircon are present in all samples.
*Average phenocryst compositions are from analogous samples of the same units published by Henshaw (2002).

chemistry is also characteristic of tuff units in other parts of the SRP (e.g. central SRP Cougar Point Tuff units; Cathey & Nash, 2004).

Low-$\delta^{18}O$ Kilgore Tuff and post-Kilgore rhyolites

The Kilgore Tuff is moderately to densely welded with ~1–10 vol. % phenocrysts (Table 2). Plagioclase phenocrysts (average composition of $Ab_{67}An_{25}Or_8$; Table 2; Supplementary Data Table 2) do not typically exhibit core–rim zoning, nor form crystal clusters with quartz, but rarely, alkali feldspar overgrowth rims surround plagioclase cores. Very commonly, small (≤1 mm), anhedral–subhedral clinopyroxene and orthopyroxene crystals are attached to larger plagioclase phenocrysts (Fig. 4c). Some clinopyroxene crystals possess sieved cores and homogeneous rims. However, we found no appreciable core–rim zoning in either isolated crystals or glomerocrysts and the average orthopyroxene and clinopyroxene compositions are $En_{38}Fs_{58}Wo_4$ and $En_{28}Fs_{32}Wo_{40}$, respectively (Table 2; Supplementary Data Table 2). Three Kilgore Tuff samples (06HS-10, 06HS-11, 95-2017b) contain anhedral clinopyroxene crystals with simple twins that are petrographically similar to twinned clinopyroxene crystals observed in the Blacktail Creek Tuff (Fig. 4g and h). Magnetite and ilmenite constitute ~1–2 vol. % of the total phenocryst content and are often present in glomerocrystic clusters of plagioclase and pyroxene. The average Fe–Ti oxide temperature obtained from single magnetite–ilmenite pairs in the Kilgore Tuff is 856°C (see 'Magmatic temperatures' section; Henshaw, 2002). Zircon (~50–120 μm) is commonly attached to or included within larger magnetite crystals.

Post-Kilgore lavas range from glassy and nearly aphyric (~1–2 vol. % phenocrysts) to porphyritic (~20 vol. % phenocrysts) (Table 2). Average plagioclase compositions of post-Kilgore lavas are similar to those of the Kilgore Tuff (Table 2; Appendix A; Supplementary Data Table 2). A few plagioclase crystals with alkali feldspar overgrowth rims were found in the post-Kilgore Indian Creek rhyolite (e.g. Fig. 4e), but typically plagioclase is isolated and unzoned. As in the Kilgore tuff, orthopyroxene and clinopyroxene commonly occur in crystal clusters with plagioclase (Fig. 4c–f). Average orthopyroxene and clinopyroxene compositions of post-Kilgore rhyolites are nearly identical to those of the Kilgore tuff, with the exception of the Juniper Buttes rhyolite, which are slightly less evolved (Table 2). Thus, it appears that post-Kilgore lavas generally have similar phenocryst sizes, morphologies and compositions to the Kilgore Tuff.

Overall, the mineralogy of the low-$\delta^{18}O$ Kilgore Tuff and post-Kilgore lavas is similar to that of the normal-$\delta^{18}O$ Heise tuff units that preceded them (Tables 1 and 2). All units lack amphibole and biotite, and the

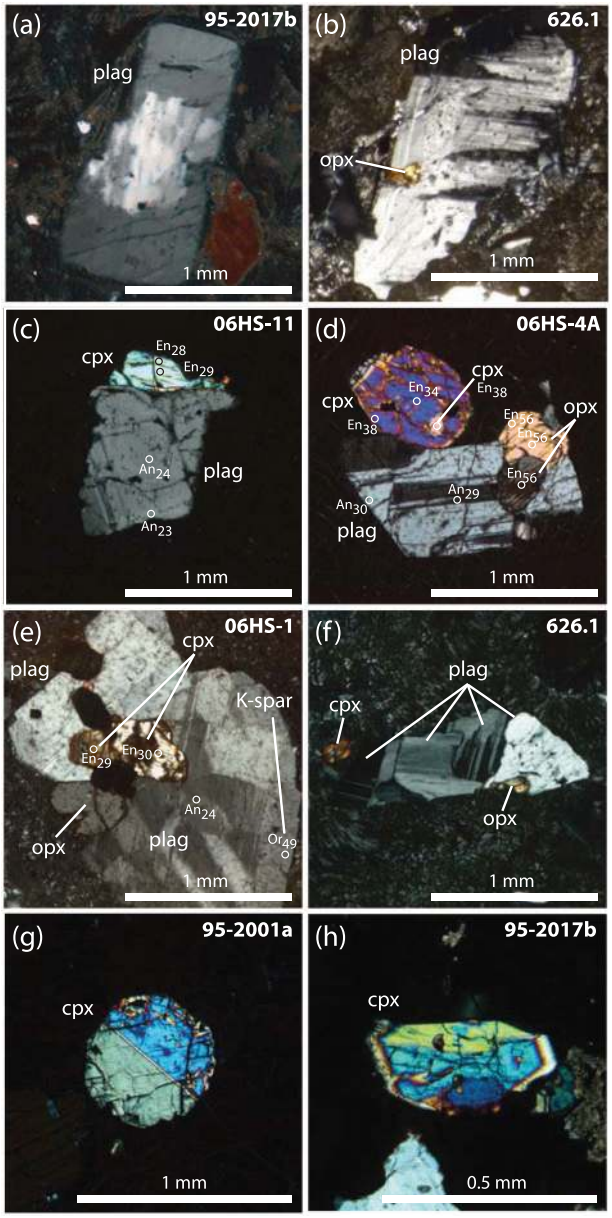

Fig. 4. Photomicrographs of Heise rhyolites in cross-polarized light. plag, plagioclase; opx, orthopyroxene; cpx, clinopyroxene; K-spar, alkali feldspar. Electron microprobe analyses of mineral compositions are indicated in mole fractions of anorthite (An) for plagioclase, enstatite (En) for orthopyroxene and clinopyroxene, and orthoclase (Or) for alkali feldspar. (a) Anhedral plag core with euhedral overgrowth rim. (b) Sieved plag core with opx inclusion. (c) Plag and cpx crystal cluster; crystals do not exhibit significant core–rim zoning. (d) Plag, opx and cpx crystal cluster; crystals do not exhibit significant core–rim zoning. (e) Plag, opx and cpx crystal cluster; plag crystal on the right has a K-spar overgrowth rim. (f) Plag, opx and cpx crystal cluster. (g) Twinned cpx crystal. (h) Twinned cpx crystal.

presence or absence of quartz appears to be related to the total crystal content and not the chemical compositions of the rhyolites (Tables 2 and 3). Mineral compositions of normal-$\delta^{18}O$ and low-$\delta^{18}O$ Heise units generally overlap, and although some units define distinct compositional fields (particularly for orthopyroxene; Appendix A); these differences do not correspond in any systematic way to $\delta^{18}O$ variations. However, we observe that only the Kilgore Tuff and Blacktail Creek Tuff have clinopyroxene crystals with simple twins (Fig. 4g and h), and only the low-$\delta^{18}O$ Kilgore Tuff and post-Kilgore rhyolites have glomerocrystic clusters of plagioclase, orthopyroxene and clinopyroxene (Fig. 4c–f).

WHOLE-ROCK GEOCHEMISTRY

Major elements

The majority of Heise rhyolites are peraluminous to metaluminous high-silica rhyolites with 75–77 wt % SiO_2, 12–13 wt % Al_2O_3, 0·4–0·9 wt % CaO, 1–2 wt % FeO and 0·1–0·3 wt % MgO (Table 3). These compositions are identical to those of high-silica rhyolites erupted in the neighboring Yellowstone Plateau volcanic field with respect to many major element concentrations and ratios; for example, low CaO and MgO and high K/Na ratios (Hildreth *et al.*, 1984; Christiansen, 2001). They are also similar to those of high-silica rhyolites of the Bruneau–Jarbidge volcanic field in the central SRP, based on common rhyolite classification indexes such as K_2O/Na_2O and molar $Al_2O_3/(CaO+Na_2O+K_2O)$ (Bonnichsen *et al.*, 2008). Most Heise tuff units that preceded the low-$\delta^{18}O$ Kilgore tuff and post-Kilgore rhyolites have lower SiO_2 and higher FeO and MgO concentrations, indicating that they are less evolved (Table 3). These include the Blacktail Creek Tuff, the Conant Creek Tuff, and the Pre-Kilgore Tuff, which have ~71–74 wt % SiO_2, ~2–4 wt % FeO and ~0·3–1 wt % MgO (Table 3). The more evolved, low-$\delta^{18}O$ Kilgore Tuff and post-Kilgore rhyolites have major element compositions that overlap, reflecting the similar mineralogy and mineral chemistry described above for these units.

When whole-rock normative compositions are plotted in the Ab–Or–Qtz system, rhyolites from the Kilgore cycle plot between the 1 kbar and 2 kbar cotectic curves near the ternary minima (Fig. 5). The normative compositions of the Kilgore Tuff and post-Kilgore rhyolites are similar to those of the Blacktail Creek Tuff and Walcott Tuff (Fig. 5). All Heise rhyolites plot within or near the locus of most granite compositions (gray field in Fig. 5), and represent near-eutectic liquids at the low pressure–temperature minimum (i.e. 'granite minimum') of the Ab–Or–Qtz system. The average normative compositions of the Yellowstone and Bruneau–Jarbidge rhyolites are similar to those of the Heise rhyolites, but the Yellowstone rhyolites have a larger proportion of normative Qtz and Bruneau–

Table 3: Major and trace element compositions of Heise samples

Sample:	95-2001a	06HS-18	08HS-10	06HS-16	06HS-5	06HS-14	TNP96-43	95-2017b	95-2015	06HS-10	06HS-11	95-2010	06HS-4A	626.1	06HS-1	06HS-19
Unit:	Blacktail Creek Tuff	Walcott Tuff	Lidy Hot Springs rhyolite	Wolverine Creek Tuff	Conant Creek Tuff	Pre-Kilgore Tuff	Kilgore Tuff	Kilgore Tuff	Kilgore Tuff	Kilgore Tuff	Kilgore Tuff	Kilgore Tuff	Juniper Buttes rhyolite	Long Hollow rhyolite	Indian Creek rhyolite	Sheridan Reservoir rhyolite[1]
Map ID:	BCT	WT	LHS	WCT	CCT	KT #1	KT #4	KT #2	KT #3	KT #1	KT #1	KT #1	JB	LH	IC	SR
Lat. (°N):	43·51	43·81	44·13	43·53	43·32	43·53	43·86	44·13	44·35	43·53	43·53	43·53	44·06	43·71	44·29	44·46
Long. (°W):	111·76	112·84	112·54	111·70	111·14	111·70	110·56	112·54	112·17	111·70	111·70	111·70	111·84	111·53	112·41	111·68
Major element analyses by XRF (wt %)																
SiO_2	74·40	75·49	76·67	75·81	74·26	70·78	75·75	76·01	76·42	75·95	75·90	76·13	76·32	76·31	75·27	75·85
TiO_2	0·31	0·22	0·30	0·17	0·21	0·55	0·28	0·24	0·23	0·24	0·24	0·24	0·24	0·23	0·25	0·26
Al_2O_3	13·14	12·03	12·31	12·60	14·17	15·86	12·48	12·30	12·29	12·49	12·17	12·23	12·58	12·39	12·82	12·17
FeO*	1·95	1·27	1·17	1·65	2·07	3·93	2·14	1·67	1·69	1·79	1·93	1·73	1·26	1·40	1·88	2·48
MnO	0·05	0·03	0·04	0·04	0·04	0·10	0·02	0·04	0·03	0·04	0·04	0·04	0·02	0·03	0·03	0·05
MgO	0·31	0·28	0·13	0·33	0·74	1·11	0·09	0·19	0·08	0·15	0·20	0·15	0·19	0·22	0·17	0·06
CaO	1·22	2·11	0·58	0·87	1·06	1·20	0·48	0·81	0·44	0·69	0·86	0·70	0·76	0·66	0·48	0·63
Na_2O	3·30	3·45	3·40	3·28	2·08	2·54	3·53	3·06	3·60	3·07	3·27	3·20	2·71	3·36	3·51	3·70
K_2O	5·27	5·09	5·38	5·20	5·36	3·84	5·19	5·65	5·19	5·55	5·36	5·55	5·90	5·34	5·32	4·78
P_2O_5	0·04	0·03	0·02	0·04	0·02	0·09	0·04	0·03	0·03	0·03	0·03	0·03	0·02	0·06	0·28	0·02
Trace element analyses by XRF (ppm)																
Ba	1099	914	840	573	509	974	1063	832	973	876	878	815	894	774	1061	2010
Rb	174	171	181	165	147	114	184	176	175	162	162	174	198	189	156	143
Sr	84	39	29	40	25	82	34	32	28	26	27	25	40	33	34	61
Zr	327	221	239	185	273	538	395	301	325	312	310	324	203	224	332	462
Y	44	54	52	75	77	78	56	56	52	63	63	57	47	52	65	65
Nb	32	41	41	54	56	50	48	47	49	48	48	47	37	42	50	36
Ga	18	17	17	22	22	24	20	19	20	20	19	20	17	20	19	20
Zn	61	41	45	86	90	116	63	72	57	60	75	61	38	48	62	91
Pb	26	23	25	28	26	28	25	24	23	25	29	26	24	27	27	29
La	66	71	67	78	81	75	89	84	85	81	79	83	69	81	87	79
Ce	120	136	126	154	159	160	161	157	146	156	161	163	128	142	160	123
Th	27	26	28	25	26	26	26	26	27	26	26	26	28	29	26	21
Nd	45	54	48	61	65	63	68	61	61	58	64	61	44	56	60	66
U	7	7	9	6	5	5	7	7	6	7	6	6	6	8	5	5
Ni	4	3	0	5	2	7	4	4	4	3	0	4	4	3	7	4
Cu	1	5	0	5	4	10	3	4	2	5	23	2	4	4	7	7
Cr	2	2	1	8	5	13	3	2	1	3	6	2	4	4	9	5
Sc	5	3	3	2	3	9	4	4	4	4	4	5	3	3	3	4
V	9	24	2	9	2	31	7	6	4	4	5	5	6	6	6	1

[1]Post-Huckleberry Ridge Tuff unit (see text for details).
*All Fe given as FeO.
Samples are normalized to 100% anhydrous. Map ID corresponds to labels in Fig. 1.

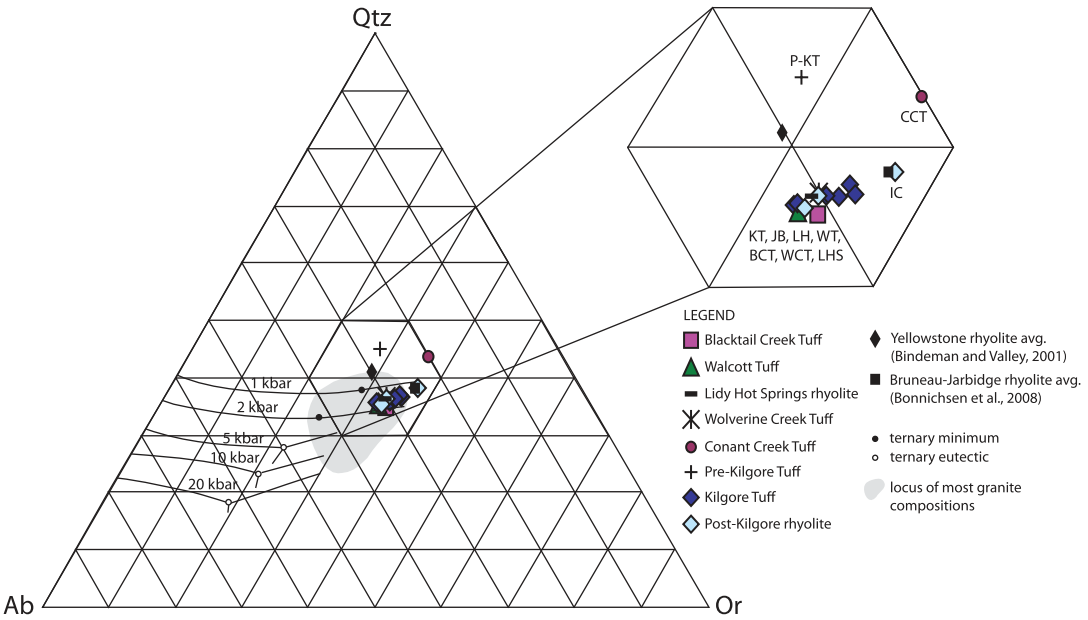

Fig. 5. Heise whole-rock normative (CIPW) rhyolite compositions plotted in the albite (Ab)–orthoclase (Or)–quartz (Qtz) system. Heise units are shown by the symbols (see legend) and labels (BCT, Blacktail Creek Tuff; WT, Walcott Tuff, LHS, Lidy Hot Springs rhyolite; WCT, Wolverine Creek Tuff; CCT, Conant Creek Tuff; P-KT, Pre-Kilgore Tuff; KT, Kilgore Tuff; JB, Juniper Buttes rhyolite; LH, Long Hollow rhyolite; IC, Indian Creek rhyolite). Ternary cotectic curves and eutectic minima from 20 kbar to 1 kbar are shown (Wyllie *et al.*, 1976). The gray shaded field represents the composition of most granites. Heise rhyolite compositions plot near the low-pressure (1–2 kbar) ternary minimum. The average normative compositions of Yellowstone and Bruneau–Jarbidge rhyolites are also shown. The CCT and P-KT units, which plot outside the compositional field of the other Heise units, have relatively low unnormalized major oxide totals but are petrographically fresh and unaltered in hand sample and thin section.

Jarbidge rhyolites have a lower proportion of normative Ab (Fig. 5).

Trace elements

Concentrations of the large ion lithophile element (LILE) Ba, and the high field strength elements (HFSE) Y, Nb, La, Ce and Nd, reveal temporal trends that define the compositional evolution of the Heise eruptions. In successive eruptions of the Blacktail Creek Tuff, Walcott Tuff, Wolverine Creek Tuff, and Conant Creek Tuff, Ba progressively decreases, whereas Y, Nb, La, Ce and Nd progressively increase (Table 3). Magmas belonging to the last low-$\delta^{18}O$ Kilgore cycle (4·87–3·96 Ma) have trace element concentrations that are similar to those of the initial Blacktail Creek Tuff eruption.

To investigate the role of fractional crystallization in the temporal variations observed for Heise trace element concentrations, we chose the trace element ratios Rb/Sr and Rb/Ba to assess plagioclase fractionation (removal of Sr and Ba relative to Rb), and Zr/Nb, La/Nb and Ce/Nb to assess clinopyroxene and zircon fractionation (removal of Zr, La and Ce relative to Nb). Rb/Sr and Rb/Ba ratios define an increasing trend for successive Heise eruptions from 6·62 to 5·51 Ma, a sharp decrease with the appearance of the low-$\delta^{18}O$ Pre-Kilgore Tuff at 4·87 Ma, an increase with the low-$\delta^{18}O$ Kilgore Tuff at 4·45 Ma, and a slight decrease with the low-$\delta^{18}O$ post-Kilgore lavas from 4·29 to 3·96 Ma (Fig. 6a and b). Zr/Nb, La/Nb and Ce/Nb ratios reveal a similar temporal pattern (in reverse), with a negative trend for successive Heise eruptions from 6·62 to 5·51 Ma, followed by an increase in the low-$\delta^{18}O$ Pre-Kilgore Tuff at 4·87 Ma, and relatively constant ratios for all low-$\delta^{18}O$ Kilgore Tuff and post-Kilgore units from 4·45 to 3·96 Ma (Fig. 6c–e). Although zoning is present within single Heise tuff units (Morgan, 1988), all available trace element data (Morgan, 1988; Morgan & McIntosh, 2005) indicate that the ranges of concentrations within each tuff are not sufficiently broad to obscure the temporal trends that we observe (e.g. gray shaded fields in Fig. 6c).

Although the Rb/Sr ratios of the Heise rhyolites (~1–7; Fig. 6a) are not nearly as high as those determined for interstitial Yellowstone rhyolite glasses (up to 140; Vazquez & Reid, 2002), or extreme cases found in large-volume rhyolites elsewhere (e.g. up to 2000 for Long Valley rhyolites; Halliday *et al.*, 1989), when combined with other trace element ratios (Fig. 6b–e), they provide a compelling case for small degrees (~10–15%) of fractional crystallization of plagioclase (~9–13%), clinopyroxene (~1–2%) and zircon (<1%) from a common rhyolite parent to generate the normal-$\delta^{18}O$ Blacktail Creek Tuff, Walcott Tuff and Conant Creek Tuff (Appendix B). This was followed by tapping of a

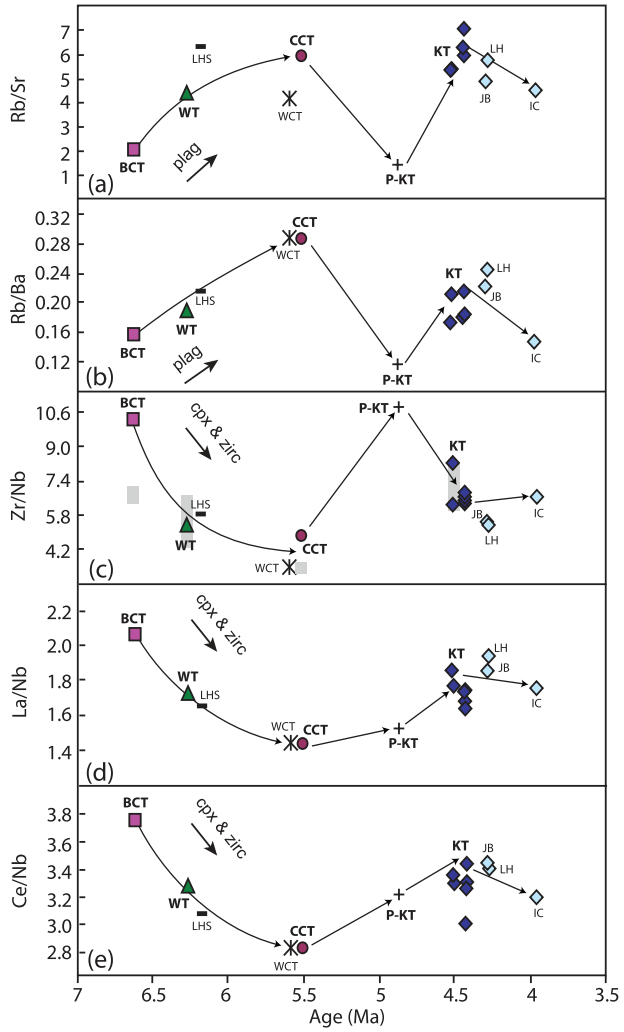

Fig. 6. Temporal variations in trace element ratios of Heise rhyolites. Heise units are indicated by the same symbols and labels as used in Fig. 5. Continuous lines in (a)–(e) show the temporal evolution in trace element ratios for successive Heise eruptions. The gray shaded fields in (c) show the ranges of trace element ratios published by Morgan & McIntosh (2005) for single Heise tuff units. Fractional crystallization of plagioclase (plag), clinopyroxene (cpx) and zircon (zirc) from a common source at ~6·6–5·5 Ma, followed by tapping of a less evolved source at ~4·9 Ma to generate the final Kilgore-cycle magmas, can explain the temporal variations observed (see text and Appendix B for details).

less evolved, Blacktail Creek Tuff-like magma at 4·87 Ma to generate the final low-$\delta^{18}O$ Kilgore cycle. The more evolved Kilgore and post-Kilgore rhyolite compositions can be generated from the less evolved Pre-Kilgore Tuff magma by ~10% fractional crystallization (Appendix B).

OXYGEN ISOTOPES

Rhyolites from the Heise volcanic field span a large (~4‰) range in magmatic $\delta^{18}O$. The climactic Kilgore Tuff is the most voluminous low-$\delta^{18}O$ magma yet discovered in the SRP and worldwide. The ~4‰ range in $\delta^{18}O$ exhibited by the Heise rhyolites is similar to those of the Yellowstone and Bruneau–Jarbidge rhyolites, and the timing and magnitude of $\delta^{18}O$ depletion in the three volcanic fields show striking parallels. A summary of our new oxygen isotope data for the Heise volcanic field, with particular emphasis on the final low-$\delta^{18}O$ Kilgore cycle, is provided below. These new data are compared with those for other volcanic centers in the SRP, including the younger Yellowstone and older Bruneau–Jarbidge centers, as well as the contemporaneous Magic Reservoir eruptive center.

Normal-$\delta^{18}O$ to low-$\delta^{18}O$ evolution in the Heise volcanic field

Volcanism began in the Heise volcanic field at 6·62 Ma with the eruption of the normal-$\delta^{18}O$ Blacktail Creek Tuff (Fig. 7b). This unit, with $\delta^{18}O_{quartz} = 6{\cdot}40‰$ and $\delta^{18}O_{zircon} = 4{\cdot}81‰$, has a calculated $\delta^{18}O_{magma}$ value of 6·6‰, which is within the range of normal-$\delta^{18}O$ SRP xenoliths and crustal basement rocks ($\delta^{18}O \approx 6{\cdot}5–8{\cdot}5‰$; Watts *et al.*, 2010). Post-Blacktail Milo Dry Farm rhyolite is also normal-$\delta^{18}O$, with $\delta^{18}O_{quartz} = 7{\cdot}46‰$ and $\delta^{18}O_{sanidine} = 6{\cdot}75‰$. Normal-$\delta^{18}O$ volcanism continued with the eruption of the Walcott Tuff ($\delta^{18}O = 6{\cdot}1‰$); however, the post-Walcott intracaldera Lidy Hot Springs rhyolite is ~2‰ depleted ($\delta^{18}O_{magma} = 4{\cdot}4‰$) relative to previous normal-$\delta^{18}O$ Heise eruptions (Fig. 7b). Subsequently erupted small-volume Kelly Canyon rhyolite and large-volume Wolverine Creek and Conant Creek tuffs have normal-$\delta^{18}O$ magmatic values of 5·9–6·5‰, although the Conant Creek Tuff is moderately (~0·1‰) depleted relative to the lower boundary of nominally normal-$\delta^{18}O$ rhyolites ($\delta^{18}O = 6‰$) (Fig. 7b).

The final caldera-forming tuff of the Heise volcanic field, the Kilgore Tuff, has extreme (~3‰) depletions from normal-$\delta^{18}O$ magmatic values, with $\delta^{18}O_{quartz} =$ 4·29–4·33‰, $\delta^{18}O_{zircon} = 1{\cdot}50–1{\cdot}61‰$, and $\delta^{18}O_{magma} =$ 3·3–3·6‰ (Fig. 7b). Samples erupted from different vents, >100 km apart, have similar phenocryst oxygen isotope values indicating that magma homogeneity was achieved prior to eruption. The Pre-Kilgore Tuff is nearly identical in $\delta^{18}O$ to the Kilgore Tuff, with $\delta^{18}O_{quartz} = 3{\cdot}29‰$, $\delta^{18}O_{zircon} = 1{\cdot}89‰$, and $\delta^{18}O_{magma} = 3{\cdot}5‰$ (Fig. 7b). We observe that a coarse lithic breccia beneath the Kilgore Tuff (stratigraphically below 06HS-10 in Fig. 3) is high-$\delta^{18}O$, with $\delta^{18}O_{quartz} \approx$ 15–16‰. In addition, lithic fragments that constitute ~1–2 vol. % of the Kilgore Tuff (06HS-11 in Fig. 3) are normal–high-$\delta^{18}O$, in nearly equal proportions of propylitically altered normal-$\delta^{18}O$ tuffs ($\delta^{18}O_{whole\ rock} \approx 7–9‰$) and high-$\delta^{18}O$ sandstone ($\delta^{18}O_{quartz} \approx 14–15‰$). Combined, this evidence argues against syneruptive modification of the Kilgore tuff to account for its low-$\delta^{18}O$ signature (see Garcia *et al.*, 1998). Smaller volume effusive post-Kilgore Tuff lavas and domes

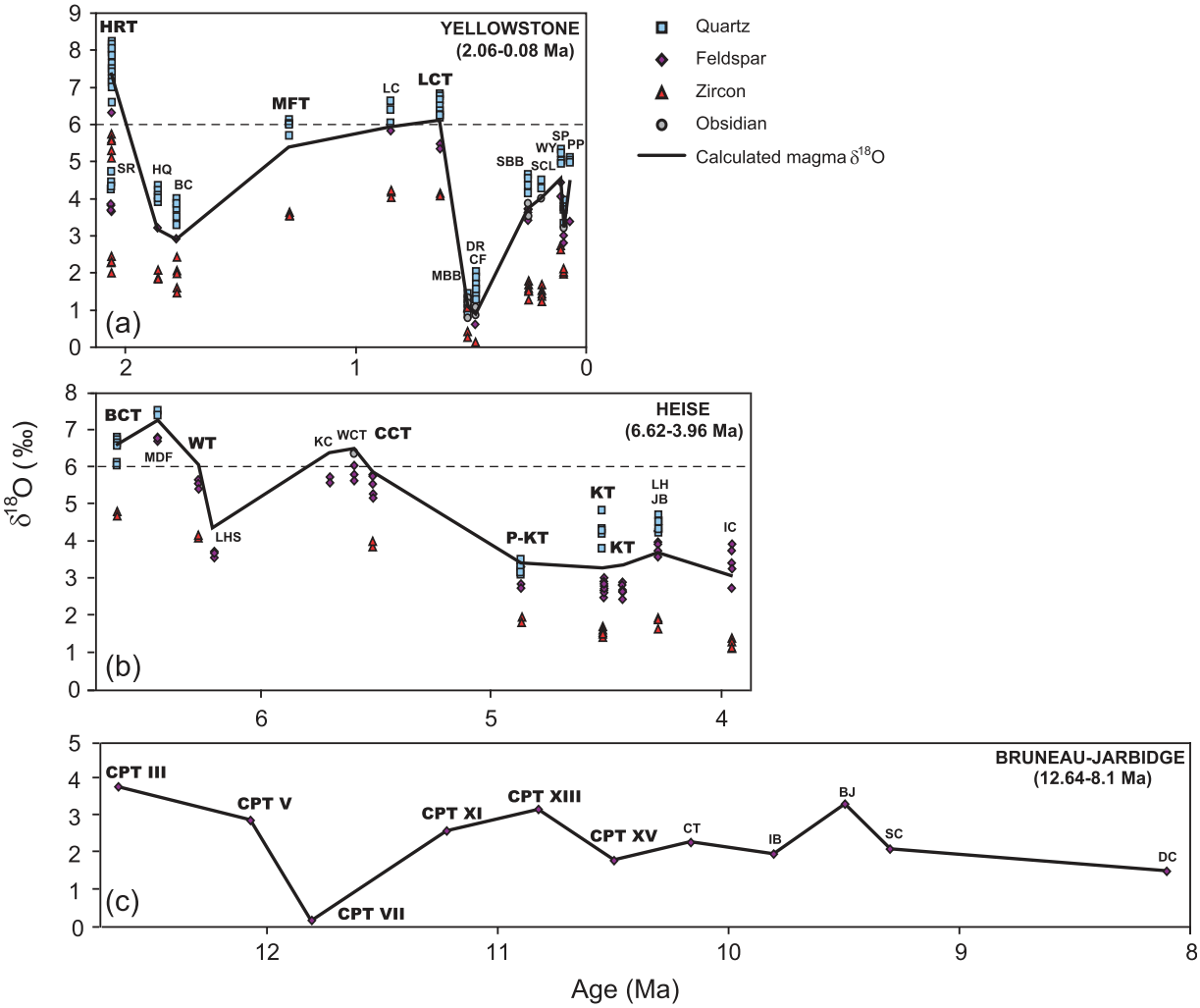

Fig. 7. Temporal variations in oxygen isotope compositions of Yellowstone (a), Heise (b) and Bruneau–Jarbidge (c) rhyolites. Major caldera-forming tuff units are indicated with bold labels. Phenocryst oxygen isotope analyses obtained by laser fluorination are shown by the symbols. Yellowstone data are from Bindeman & Valley (2001) and Bruneau–Jarbidge data are from Bonnichsen *et al.* (2008). (See Table 1 and the online Supplementary Data Table 3 for the Heise $\delta^{18}O$ data.) Calculated magma $\delta^{18}O$ values for successive rhyolite eruptions are connected by continuous black lines. The fine dashed black lines in (a) and (b) show the lower limit of normal-$\delta^{18}O$ rhyolites ($\delta^{18}O = 6‰$). The remarkable similarities should be noted in the timing and magnitude of $\delta^{18}O$ depletion and recovery in (a) and (b), which are synchronous with caldera collapse events (see text for detailed discussion).

are equally low in $\delta^{18}O$, but encompass a slightly larger $\delta^{18}O$ range than the Kilgore Tuff (Fig. 7b). The Juniper Buttes resurgent dome and Long Hollow rhyolite are ~0·1–0·4‰ elevated from the 3·3–3·6‰ range of the Pre-Kilgore Tuff and Kilgore Tuff. The later Indian Creek rhyolite is ~0·3–0·6‰ lower in $\delta^{18}O$, with $\delta^{18}O_{magma} = 3·0‰$.

Oxygen isotope compositions of zircon and single phenocrysts

An interesting result of oxygen isotopic investigation in the Heise volcanic field is that despite $\delta^{18}O$ homogeneity of the Kilgore Tuff on the caldera-wide scale in major phenocrysts, it preserves remarkable $\delta^{18}O$ heterogeneity in accessory zircon. Whereas we find that laser fluorination $\delta^{18}O$ analyses of single phenocrysts of quartz and sanidine and bulk zircon are reproducible within a standard error of less than ~0·1‰ (Table 1), a subset of analyses obtained by ion microprobe for single Kilgore Tuff zircons reveal significant $\delta^{18}O$ heterogeneity (Table 4). These zircon $\delta^{18}O$ values are almost exclusively low, ranging from −1·30‰ to 3·03‰, with the exception of one zircon crystal that has a normal-$\delta^{18}O$ value of 6·07‰ (Fig. 8). The average $\delta^{18}O$ value for zircons analyzed by ion microprobe is nearly identical to the average $\delta^{18}O$ value for bulk zircons analyzed by laser fluorination (Fig. 8). Single zircons from the Pre-Kilgore Tuff are also low-$\delta^{18}O$, and overlap with the Kilgore tuff zircons (Fig. 8), but we note that for the Pre-Kilgore

Table 4: Oxygen isotopic compositions and U–Pb ages determined by ion microprobe

Sample	U–Pb age (Ma)	1σ (Ma)	$\delta^{18}O$ (‰)	1σ ext (‰)	Av. $\delta^{18}O$ (‰)
HS-14_PKT_g3	4·40	0·33	1·06	0·22	2·84
HS-14_PKT_g4	4·23	0·50	1·96	0·22	
HS-14_PKT_g5	4·90	0·37	0·92	0·22	
HS-14_PKT_g6	4·78	0·59	2·45	0·22	
HS-14_PKT_g7	5·19	0·24	0·89	0·22	
HS-14_PKT_g8	4·96	0·31	5·45	0·22	
HS-14_PKT_g9	5·07	0·30	4·96	0·22	
HS-14_PKT_g10	4·68	0·23	5·02	0·22	
HS-10_Kilg_g1	4·25	0·35	−0·40	0·22	1·30
HS-10_Kilg_g2	4·50	0·28	0·97	0·22	
HS-10_Kilg_g3	5·08	1·16	2·65	0·22	
HS-10_Kilg_g4	4·30	0·26	3·03	0·22	
HS-10_Kilg_g5	4·95	0·26	−0·59	0·22	
HS-10_Kilg_g6	4·50	0·33	2·76	0·22	
HS-10_Kilg_g7	4·84	0·34	−0·68	0·22	
HS-10_Kilg_g8	4·09	0·30	2·78	0·22	
HS-10_Kilg_g9	5·06	0·27	1·22	0·22	
HS-11_Kilg_g1	4·72	0·23	1·04	0·22	1·28
HS-11_Kilg_g2	4·73	0·30	0·46	0·22	
HS-11_Kilg_g3	4·37	0·61	−0·76	0·22	
HS-11_Kilg_g4	4·92	0·36	2·80	0·22	
HS-11_Kilg_g5	4·35	0·28	−1·30	0·22	
HS-11_Kilg_g6	4·44	0·27	0·81	0·22	
HS-11_Kilg_g7	4·70	0·32	0·96	0·22	
HS-11_Kilg_g9	4·57	0·29	6·07	0·22	
HS-11_Kilg_g10	4·63	0·30	1·40	0·22	

Single spot analyses of single zircon cores by ion microprobe. Errors for oxygen isotopic compositions (1σ ext) are the external errors of KIM-5 zircon standards and are corrected for minor instrumental drift (~0.3‰ over 9 h analysis duration). The average oxygen isotopic compositions in the rightmost column are averages of single analyses for the Pre-Kilgore Tuff (HS-14, $n=8$) and Kilgore Tuff (HS-10, $n=9$; HS-11, $n=9$).

Tuff, the average of single zircon analyses obtained by ion probe is ~1‰ higher than the bulk zircon average obtained by laser fluorination. The fact that the Pre-Kilgore Tuff zircons have U–Pb ages that are ~300 kyr older and slightly higher in $\delta^{18}O$ than the Kilgore Tuff (Fig. 8), may indicate the progress of (incomplete) zircon annealing via solution–reprecipitation in the early stages of Kilgore Tuff magma formation.

Laser fluorination oxygen isotope data and published mineral pair fractionation factors for quartz–zircon (Trail *et al.*, 2009) and quartz–K-feldspar (Zheng, 1993) are consistent with high-temperature oxygen isotopic equilibrium for the Heise rhyolites (Fig. 9a and b). This is in contrast to the strong O-isotope disequilibria that have been documented for many Yellowstone rhyolites (Fig. 9a and b; Bindeman & Valley, 2001; Bindeman *et al.*, 2008). However, as indicated by our ion microprobe data for the Kilgore Tuff and Pre-Kilgore Tuff, single zircons preserve significant $\delta^{18}O$ heterogeneity, and require zircon crystallization from multiple, independent magma batches with unique low-$\delta^{18}O$ values (Fig 8). Because the $\delta^{18}O$ averages of single zircon analyses by ion microprobe match the $\delta^{18}O$ values of bulk zircons obtained by laser fluorination for Kilgore Tuff samples erupted >100 km apart (Table 1; Fig. 7b), and presumably from different parts of the Kilgore magma chamber based on their locations relative to proposed Kilgore Tuff vent sources (Morgan & McIntosh, 2005; Fig. 1), it is evident that a heterogeneous zircon crystal cargo was convectively distributed (averaged) over great lateral distances prior to eruption of the Kilgore Tuff magma.

The zircon $\delta^{18}O$ heterogeneity that we report for the low-$\delta^{18}O$ Kilgore Tuff ($\delta^{18}O$ range of −1·3‰ to 6·1‰) is analogous to the oxygen isotope heterogeneity reported by Cathey *et al.* (2008) for single zircons of the low-$\delta^{18}O$ Bruneau–Jarbidge tuffs ($\delta^{18}O$ range of −3·1‰ to 6·4‰) and that reported by Bindeman *et al.* (2008) for single zircons of low-$\delta^{18}O$ rhyolites from the Yellowstone volcanic field ($\delta^{18}O$ range of −2·2‰ to 7·6‰). This means that all of the voluminous low-$\delta^{18}O$ SRP rhyolites that have been studied thus far contain zircon crystals with diverse $\delta^{18}O$ values. Furthermore, it is evident that assembly of large-volume low-$\delta^{18}O$ magmas with diverse zircon populations can occur rapidly, within error of U–Pb zircon dating (hundreds of thousands of years).

Comparison with the Yellowstone Plateau volcanic field

Like Heise, volcanism in the Yellowstone Plateau volcanic field began with the eruption of a normal-$\delta^{18}O$ caldera-forming tuff, the 2·06 Ma Huckleberry Ridge Tuff ($\delta^{18}O_{magma}=7·0–7·5‰$) (Fig. 7a). Following the Huckleberry Ridge Tuff eruption, the oxygen isotope trend plunges sharply with the appearance of several low-$\delta^{18}O$ post-Huckleberry Ridge Tuff rhyolites, including the Headquarters flow ($\delta^{18}O_{magma}=3·2‰$) and Blue Creek flow ($\delta^{18}O_{magma}=2·9‰$) (Fig. 7a). The Sheridan Reservoir rhyolite has an age and $\delta^{18}O$ composition that overlaps these post-Huckleberry Ridge Tuff units ('SR' in Fig. 7a), supporting our interpretation that it is a post-Huckleberry Ridge Tuff rather than a post-Kilgore unit. Low-$\delta^{18}O$ post-Huckleberry Ridge Tuff rhyolites, which erupted ~0·2–0·4 Myr after the first phase of normal-$\delta^{18}O$ eruptions and have depletions of ~3–4‰ from normal-$\delta^{18}O$ values, were comparable in timing and $\delta^{18}O$ depletion with the first low-$\delta^{18}O$ rhyolite in the

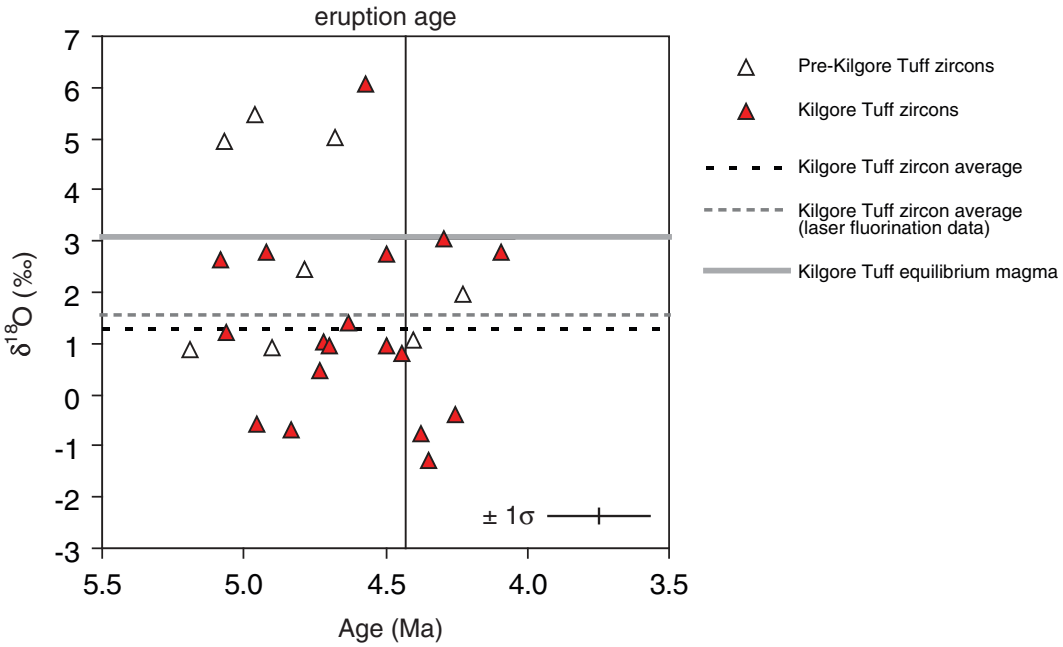

Fig. 8. Ion microprobe oxygen isotope data for single zircon crystals from the Kilgore Tuff and Pre-Kilgore Tuff. Oxygen isotope compositions are plotted against U–Pb age for single zircon spots. (See Table 4 for the $\delta^{18}O$ and U–Pb data.) The average 1σ error for $\delta^{18}O$ values and U–Pb ages is shown in the bottom right corner. The continuous vertical line is the Ar–Ar eruption age for Kilgore Tuff samples 06HS-l0 and 06HS-l1 (4·43 Ma; Table 1). The average zircon $\delta^{18}O$ composition of the Kilgore Tuff by ion microprobe (black dashed line), equilibrium magma value for the ion microprobe zircon average (continuous gray line), and laser fluorination zircon average (dashed gray line) are included in the plot.

Heise volcanic field (Lidy Hot Springs rhyolite) (Fig. 7a and b). Like Heise, $\delta^{18}O$ values at Yellowstone recovered after the first appearance of low-$\delta^{18}O$ rhyolites by ~2–3‰ over a period of ~1 Myr, with the eruptions of the Mesa Falls Tuff ($\delta^{18}O_{magma} = 5{\cdot}4‰$), the Lewis Canyon rhyolite ($\delta^{18}O_{magma} = 5{\cdot}9‰$) and the Lava Creek Tuff ($\delta^{18}O_{magma} = 5{\cdot}9–6{\cdot}3‰$) (Fig. 7a). Post-Lava Creek Tuff rhyolites, including the Upper Basin Member ($\delta^{18}O_{magma} = 0{\cdot}7–1{\cdot}1‰$) and Central Plateau Member ($\delta^{18}O_{magma} = 3{\cdot}2–4{\cdot}5‰$) units, constitute the final pulse of low-$\delta^{18}O$ volcanism in the Yellowstone Plateau volcanic field. This final, low-$\delta^{18}O$ pulse at Yellowstone is analogous to the final, low-$\delta^{18}O$ Kilgore Tuff and post-Kilgore eruptions at Heise in terms of timing (~2 Myr after the initiation of normal-$\delta^{18}O$ volcanism), magnitude of $\delta^{18}O$ depletion (~3‰ depleted relative to normal-$\delta^{18}O$ tuffs), and duration of low-$\delta^{18}O$ eruptions (~0·5–0·9 Myr) (Fig. 7a and b).

Comparison with the Bruneau–Jarbidge volcanic field

Unlike Heise and Yellowstone, volcanic eruptions in the Bruneau–Jarbidge volcanic field are exclusively low-$\delta^{18}O$ (Fig. 7c). However, the trend in timing and magnitude of $\delta^{18}O$ depletions in successive Bruneau–Jarbidge eruptions may bear some resemblance to the $\delta^{18}O$ trends observed for Heise and Yellowstone (Fig. 7c). Volcanism in the Bruneau–Jarbidge volcanic field began at 12·64 Ma with the eruption of the Cougar Point Tuff III ($\delta^{18}O_{magma} = 3{\cdot}8‰$) (Fig. 7c). Following this eruption, $\delta^{18}O$ values steadily decreased with eruptions of Cougar Point Tuff V ($\delta^{18}O_{magma} = 2{\cdot}9‰$) and Cougar Point Tuff VII ($\delta^{18}O_{magma} = 0{\cdot}2‰$). The ~3–4‰ depletion in $\delta^{18}O$ after 1–2 caldera-forming eruptions is consistent with Heise and Yellowstone trends (Fig. 7a–c). Oxygen isotope values recovered by ~2–3‰ over a period of ~1 Myr, with the eruptions of Cougar Point Tuffs XI ($\delta^{18}O_{magma} = 2{\cdot}6‰$) and XIII ($\delta^{18}O_{magma} = 3{\cdot}2‰$), which is also consistent with Heise and Yellowstone trends (Fig. 7a–c). Cougar Point Tuff XV ($\delta^{18}O_{magma} = 1{\cdot}1‰$) and post-Cougar Point Tuff rhyolites ($\delta^{18}O_{magma} = 1{\cdot}5–2{\cdot}3‰$) have $\delta^{18}O$ values that are ~2‰ depleted relative to Cougar Point Tuff XIII, and this too is consistent with the timing and magnitude of $\delta^{18}O$ depletions observed for the final low-$\delta^{18}O$ pulse of volcanism in the Heise and Yellowstone volcanic fields (Fig. 7a–c).

The search for normal-$\delta^{18}O$ rhyolite in the central SRP continues. We report here a new normal-$\delta^{18}O$ analysis for the Jarbidge rhyolite ($\delta^{18}O_{quartz} = 8{\cdot}44‰$), which is a 16·8–15·4 Ma large-volume lava unit (Coats *et al.*, 1977) that preceded the earliest low-$\delta^{18}O$ rhyolites in the central SRP. Although the origin of this rhyolite is due to either

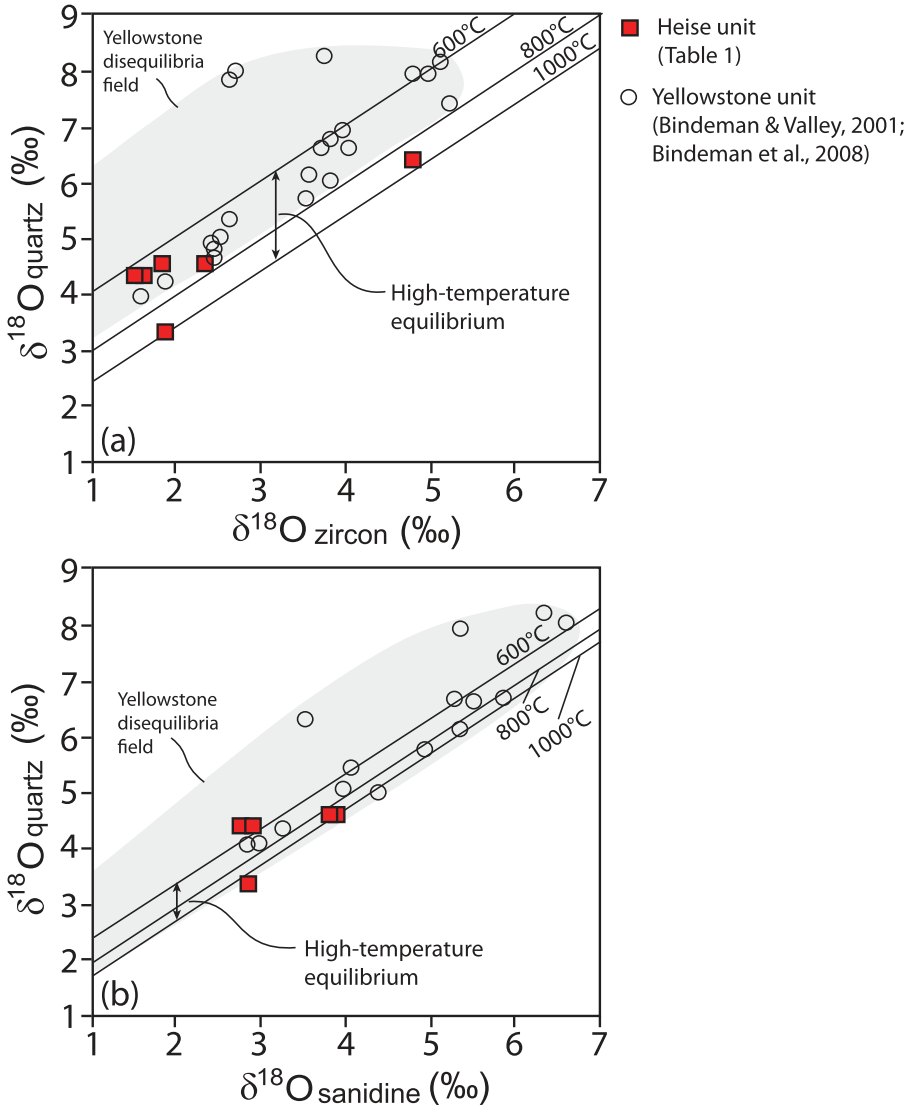

Fig. 9. $\delta^{18}O_{quartz}$–$\delta^{18}O_{zircon}$ (a) and $\delta^{18}O_{quartz}$–$\delta^{18}O_{sanidine}$ (b) showing that the Heise rhyolite units (filled squares) are in high-temperature (600–1000°C) oxygen isotopic equilibrium, in contrast to the significant disequilibria observed for Yellowstone rhyolite units (open circles and gray shaded field; Bindeman & Valley, 2001; Bindeman *et al.*, 2008). Published mineral pair fractionation factors for quartz–zircon (Trail *et al.*, 2009) and quartz–K-spar (Zheng, 1993) were used to construct the equilibrium fractionation lines that are shown in (a) and (b) for temperatures of 600°C, 800°C and 1000°C.

the SRP plume volcanism or contemporaneous northern Nevada extension, the proximity of the Jarbidge rhyolite to the Bruneau–Jarbidge volcanic field (Fig. 1 inset) combined with its age and large volume make it comparable with other rhyolites in the SRP.

Contemporaneous normal-$\delta^{18}O$ rhyolites of the Magic Reservoir Eruptive Center

We report new oxygen isotopic and whole-rock chemical data (Table 5) for the 5·8–3 Ma Magic Reservoir eruptive center in central Idaho (Fig. 1 inset). This includes small-volume (<50 km^3) ash-flow tuffs and rhyolitic domes that erupted contemporaneously with the Heise volcanic field in eastern Idaho (Fig. 1 inset). Unlike Heise, this center does not exhibit multi-cyclic calderas, permitting an independent assessment of contemporaneous rhyolitic magmatism of a different style in the SRP. Normal-$\delta^{18}O$ high-silica rhyolites of Magic Reservoir overlap the SRP continental crust in SiO_2–$\delta^{18}O$ composition, and in marked contrast to the Heise rhyolites, they span a much narrower $\delta^{18}O$ range within SiO_2–$\delta^{18}O$ compositional space (~1‰ vs ~4‰ for Heise) (Fig. 10a). The Sr and Nd isotope compositions of high-silica rhyolites of Magic Reservoir ($^{87}Sr/^{86}Sr = 0{\cdot}7109$–$0{\cdot}7242$, $^{143}Nd/^{144}Nd =$

Table 5: Locations, ages, oxygen isotopic compositions and whole-rock compositions of Magic Reservoir samples

Sample:	07MR-TF	07MR-DM2	07MR-DM3	07MR-DM4	07MR-DM1b
Description:	young tuff	Moonstone young dome	Rattlesnake young dome	Dinosaur Ridge young dome	Willow Creek young dome
Latitude (°N):	43·34	43·35	43·26	43·24	43·37
Longitude (°W):	114·40	114·46	114·35	114·34	114·57
K–Ar age (Ma):	5·6–4·8	3–4	3–4	3–4	3–4
Av. Qtz $\delta^{18}O$ (‰):	7·79	8·17	9·01	8·39	7·83
Av. Qtz cores $\delta^{18}O$ (‰):	—	8·04	8·78	8·59	8·56
Magma (‰) (calc.):	7·4	7·8	8·6	8·0	7·4
Major element analyses by XRF (wt %)					
SiO_2	75·17	69·71	76·10	—	—
TiO_2	0·26	0·69	0·06	—	—
Al_2O_3	12·81	13·66	13·24	—	—
FeO*	2·00	4·59	1·33	—	—
MnO	0·04	0·08	0·04	—	—
MgO	0·15	0·43	0·00	—	—
CaO	0·80	2·24	0·30	—	—
Na_2O	3·27	3·42	4·19	—	—
K_2O	5·49	4·96	4·73	—	—
P_2O_5	0·03	0·21	0·02	—	—
Trace element analyses by XRF (ppm)					
Ba	590	1906	19	—	—
Rb	309	103	455	—	—
Sr	71	217	6	—	—
Zr	299	713	136	—	—
Y	80	59	134	—	—
Nb	69	53	122	—	—
Ga	20	19	33	—	—
Zn	54	101	95	—	—
Pb	36	26	63	—	—
La	102	111	30	—	—
Ce	186	211	81	—	—
Th	40	13	57	—	—
Nd	69	79	29	—	—
U	12	2	20	—	—
Ni	0	0	0	—	—
Cu	5	7	0	—	—
Cr	3	3	1	—	—
Sc	4	7	1	—	—
V	8	20	6	—	—

Average $\delta^{18}O$ values for quartz (Qtz) and quartz cores. Quartz cores were obtained by air abrasion of whole quartz phenocrysts in a corundum mortar. Magma $\delta^{18}O$ values were calculated from quartz phenocryst analyses, with $\Delta^{18}O_{quartz\text{-}melt} = 0{\cdot}4‰$, applicable at liquidus temperatures of ~800°C (Bindeman & Valley, 2002). K–Ar ages are from Honjo *et al*. (1986). XRF data are normalized to 100% anhydrous with all Fe as FeO*.

0·51181–0·51208; W. P. Leeman, personal communication) indicate that they contain a significant component of Archean crust. The absence of low-$\delta^{18}O$ rhyolites in the Magic Reservoir eruptive center and the strongly radiogenic Sr and Nd isotope signatures of the Magic Reservoir rhyolites indicate partial melting of normal-$\delta^{18}O$ SRP Archean crust (Fig. 10b). By analogy with Yellowstone, the Magic Reservoir rhyolites

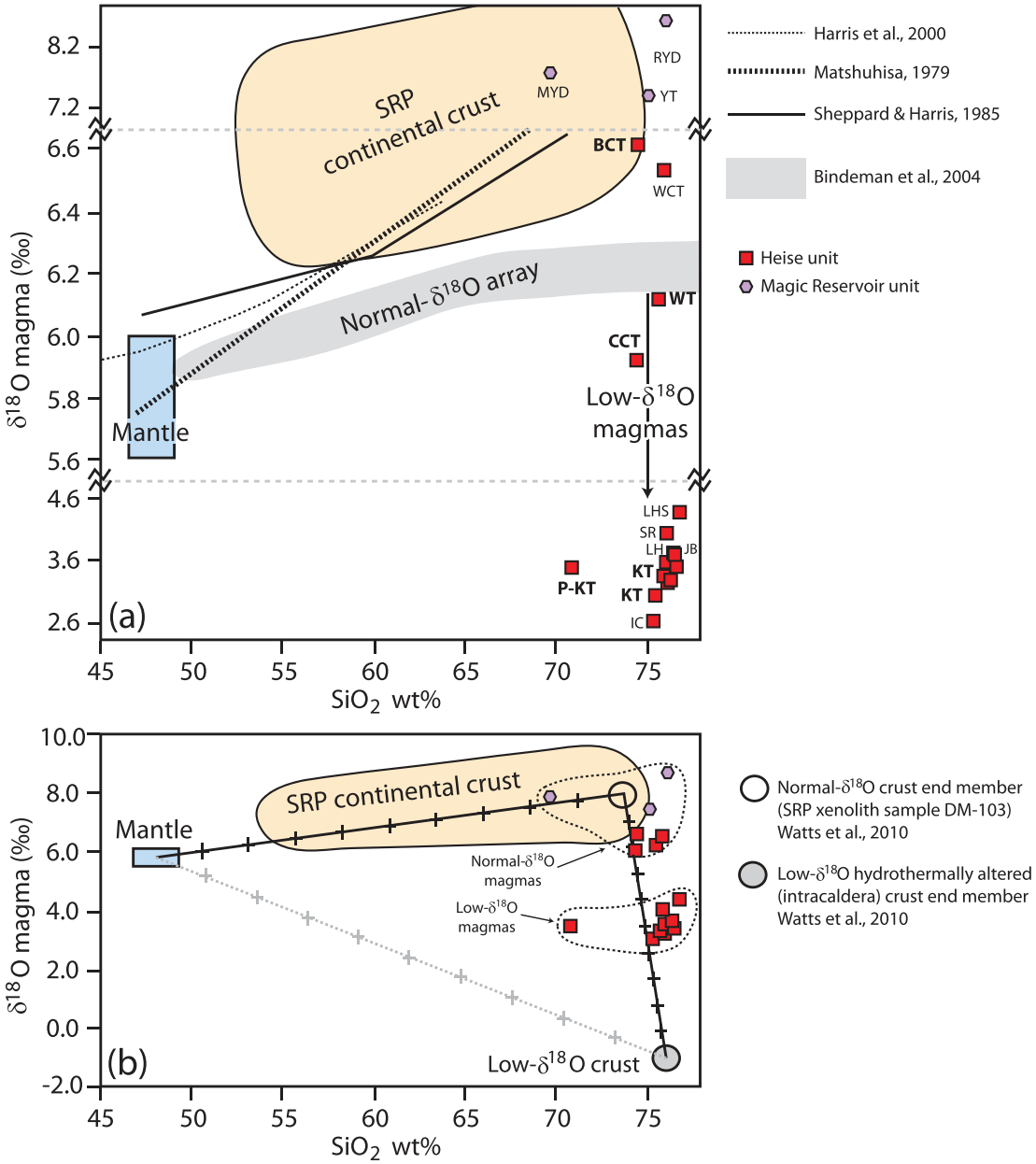

Fig. 10. $\delta^{18}O_{magma}$–SiO_2 plots showing the variation of the Heise and Magic Reservoir rhyolite units in relation to the mantle, SRP continental crust, normal-$\delta^{18}O$ differentiation trends [black lines (sources: Matsuhisa, 1979; Sheppard & Harris, 1985; Harris *et al.*, 2000) and gray field labeled 'normal-$\delta^{18}O$ array' (source: Bindeman *et al.*, 2004)] (a), and isotopic mixing of normal-$\delta^{18}O$ and low-$\delta^{18}O$ source components (b). Labels for Heise units are as in Fig. 5. Labels for Magic Reservoir units: MYD, Moonstone young dome; RYD, Rattlesnake young dome; YT, young tuff. Low-$\delta^{18}O$ Heise magmas, which lie below the normal-$\delta^{18}O$ array (a), cannot be produced by isotopic mixing of normal-$\delta^{18}O$ mantle and crust components (b). Their formation requires remelting of hydrothermally altered portions of intracaldera rock from previous Heise eruptions, with an average $\delta^{18}O$ value of ~−1‰ (b). Mixing between mantle and low-$\delta^{18}O$ crust is not confirmed by geological or geochemical evidence, and thus is tentatively indicated with a gray dashed line (b).

define a normal-$\delta^{18}O$ extracaldera trend of magma evolution (Hildreth *et al.*, 1991). This supports our view that large, multi-cyclic calderas, which are absent at Magic Reservoir but present at Heise and Yellowstone, are required for the generation of low-$\delta^{18}O$ rhyolites.

STRONTIUM AND NEODYMIUM ISOTOPES

New Sr and Nd isotope data for 13 rhyolite samples (tuffs and lavas) of the Heise volcanic field are reported in Table 1. As the Heise rhyolites were derived by melting

and hybridization of Archean crust by SRP basalt, they possess highly radiogenic $^{87}Sr/^{86}Sr$ and $^{143}Nd/^{144}Nd$ ratios that span large ranges ($^{87}Sr/^{86}Sr_i = 0{\cdot}70895$–$0{\cdot}71238$; $^{143}Nd/^{144}Nd = 0{\cdot}51214$–$0{\cdot}51233$) (Table 1; Fig. 11c and d). Successive normal-$\delta^{18}O$ Heise eruptions have $^{87}Sr/^{86}Sr$ ratios that progressively decrease and $^{143}Nd/^{144}Nd$ ratios that progressively increase (Fig. 11c and d). The trend is reversed with the eruption of the low-$\delta^{18}O$ Pre-Kilgore Tuff, which has $^{87}Sr/^{86}Sr$ and $^{143}Nd/^{144}Nd$ ratios that recover towards Blacktail Creek Tuff values (Fig. 11c and d). The low-$\delta^{18}O$ Kilgore Tuff samples have fairly constant $^{87}Sr/^{86}Sr$ and $^{143}Nd/^{144}Nd$ ratios, whereas the smaller-volume post-Kilgore rhyolites are more variable (Fig. 11c and d).

Whereas decreases in $^{87}Sr/^{86}Sr$ correspond to increases in $^{143}Nd/^{144}Nd$ in earlier Heise eruptions (6·62–4·87 Ma), we observe that for the Kilgore Tuff and post-Kilgore eruptive sequence (4·45–3·96 Ma), decreases in $^{87}Sr/^{86}Sr$ correspond to decreases in $^{143}Nd/^{144}Nd$ (Fig. 11c and d). Unlike the large variations in the Yellowstone tuffs (Fig. 11e and f), the magnitude of change of $^{87}Sr/^{86}Sr$ and $^{143}Nd/^{144}Nd$ ratios in the Kilgore and post-Kilgore eruptive sequence is small, and probably due to minor heterogeneities in the rhyolite reservoirs. Isotopic variations of Sr and Nd in the Heise rhyolites can be explained by binary mixing between Archean crust ($^{87}Sr/^{86}Sr \approx 0{\cdot}7388$, $^{143}Nd/^{144}Nd \approx 0{\cdot}5109$) and SRP basalts ($^{87}Sr/^{86}Sr \approx 0{\cdot}7063$, $^{143}Nd/^{144}Nd \approx 0{\cdot}5124$) in proportions of ~30–50% crust and ~50–70% basalt (McCurry & Rodgers, 2009; Watts *et al.*, 2010). Similar crust–basalt mixing proportions are required for the Yellowstone and Bruneau–Jarbidge rhyolites, based on the observed isotopic ranges of Sr (0·7080–0·7140) and Nd (0·5121–0·5123) (Fig. 11a–f; Hildreth *et al.*, 1991; Bonnichsen *et al.*, 2008).

The magnitude of temporal variations in Sr and Nd isotope ratios in the Heise volcanic field is intermediate between those of the older, less heterogeneous Bruneau–Jarbidge volcanic field in the central SRP and the younger, more heterogeneous Yellowstone Plateau volcanic field in the eastern SRP (Fig. 11a–f). This probably reflects the transition into thicker and more strongly radiogenic Archean terrain as volcanism progressed from west to east across the North American craton (Fig. 1 inset). However, preservation bias cannot be ruled out, in which case younger (i.e. more easterly) caldera centers may be better preserved, and thus preserve more heterogeneity, than limited exposures in older parts of the SRP.

There is no correlation between the low $\delta^{18}O$ values and high $^{87}Sr/^{86}Sr$ ratios of the Heise rhyolites, precluding the role of low-$\delta^{18}O$/high $^{87}Sr/^{86}Sr$ hydrothermal brines in low-$\delta^{18}O$ rhyolite genesis in the Heise volcanic field (see Hildreth *et al*, 1991). Compared with the heterogeneity in Sr and Nd isotope ratios in major caldera-forming tuffs at Yellowstone (Huckleberry Ridge Tuff, Lava Creek Tuff), the Sr and Nd isotope ratios of the low-$\delta^{18}O$ Heise Kilgore Tuff are much more homogeneous (Fig. 11c–f). Low-$\delta^{18}O$ post-Kilgore rhyolites of the Heise volcanic field are also more homogeneous in Sr and Nd isotope ratios than low-$\delta^{18}O$ post-Lava Creek Tuff rhyolites of the Yellowstone Plateau volcanic field (Fig. 11c–f).

MAGMATIC TEMPERATURES

Magmatic temperatures of most Heise rhyolites were within the range of 800–900°C, as determined by several independent methods (Table 1; Fig. 12). MELTS liquidus temperatures are the highest, with temperatures that are ~30° higher than zircon saturation temperatures (whole-rock) and ~80° higher than Ti-in-zircon temperatures for the same units (Fig. 12). In two cases (Conant Creek Tuff, Juniper Buttes), the Ti-in-zircon temperatures are significantly (~100–200°) lower than the calculated MELTS and zircon saturation temperatures (Fig. 12). This discrepancy is noted for many rhyolites worldwide (Fu *et al.*, 2008), and in the case of Heise may be due to uncertain Ti activities, as ilmenite and ulvöspinel compositions are not available for all units (see Wark *et al.*, 2007). Our temperature estimates for the Heise rhyolites overlap eruption temperatures determined with the Fe–Ti oxide geothermometer of Ghiorso & Sack (1991) for the Heise Blacktail Creek Tuff, Walcott Tuff, Wolverine Creek Tuff and Kilgore Tuff (734–846°C; Henshaw, 2002; Fig. 12). Liquidus temperatures of Heise rhyolites (~800–900°C) are comparable with, and in some cases higher than, those of younger rhyolites erupted in the neighboring Yellowstone Plateau volcanic field (~750–900°C; Hildreth *et al.*, 1984; Bindeman & Valley, 2001; Vazquez *et al.*, 2009) and generally lower than the older rhyolites of the Bruneau–Jarbidge volcanic field (~850–1000°C; Cathey & Nash, 2004; Nash *et al.*, 2006) (Fig. 12).

DISCUSSION

The following discussion focuses on the origin of voluminous low-$\delta^{18}O$ rhyolite magmas, based on the example of the 1800 km^3 Kilgore Tuff of the Heise volcanic field. We address the following questions: (1) How were the normal-$\delta^{18}O$ Heise tuffs that predate the low-$\delta^{18}O$ Kilgore Tuff generated? (2) What is the origin of the Kilgore Tuff's unique low-$\delta^{18}O$ signature? (3) What model of magma genesis best satisfies all available data for the Kilgore Tuff? (4) How are the low-$\delta^{18}O$ Pre-Kilgore Tuff and post-Kilgore rhyolites related to the Kilgore Tuff? In answering these questions, we highlight key similarities in the pattern of low-$\delta^{18}O$ rhyolite magma genesis at Heise, Yellowstone and Bruneau–Jarbidge, and discuss the suitability of the 4·5 Ma Kilgore Tuff as an analog for the youngest phase of voluminous rhyolitic eruptions at Yellowstone. If our interpretation for shallow (<10 km

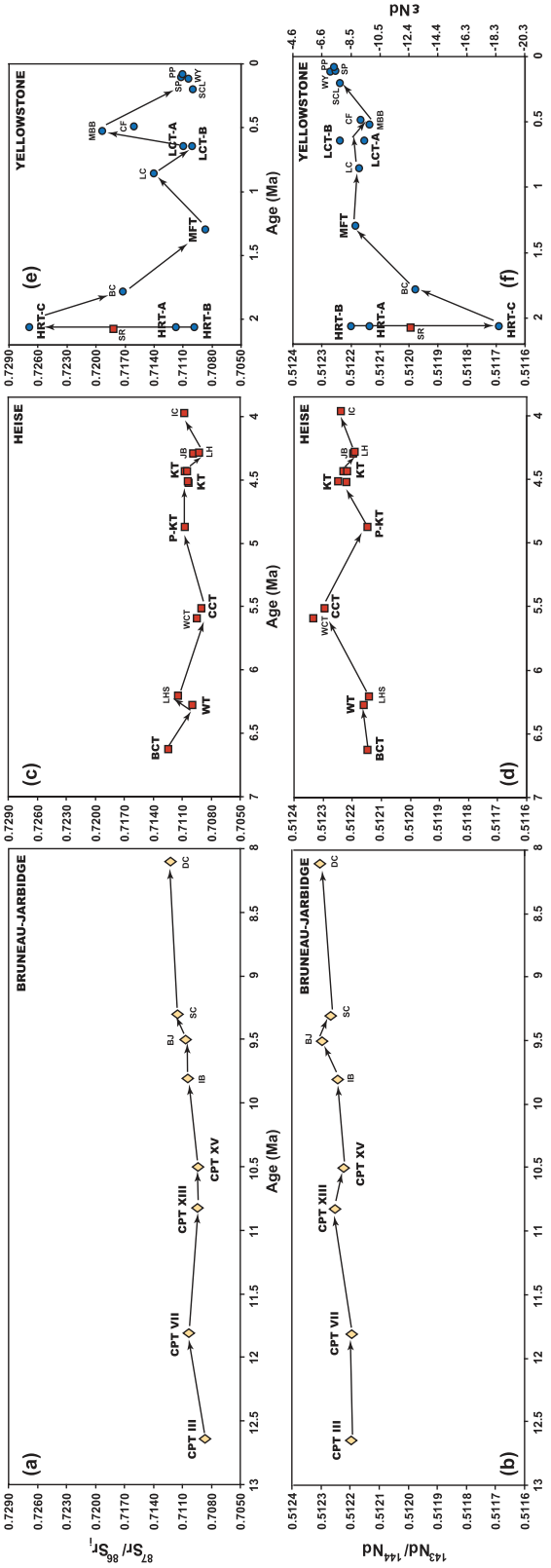

Fig. 11. Temporal variations of Sr and Nd isotope ratios in Bruneau–Jarbidge (a, b), Heise (c, d), and Yellowstone (e, f) rhyolites. Rhyolite unit labels are the same as in Fig. 7. Sr and Nd isotope data are from Bonnichsen *et al.* (2008) for Bruneau–Jarbidge rhyolites and Hildreth *et al.* (1991) and Vazquez & Reid (2002) for Yellowstone rhyolites (see Supplementary Data Table 4). It should be noted that the magnitude of the temporal variations in the Sr and Nd isotope ratios of the Heise rhyolites is intermediate between those for the older Bruneau–Jarbidge volcanic field to the west and the younger Yellowstone Plateau volcanic field to the east (Fig 1 inset). The Sheridan Reservoir rhyolite (SR; filled square) is included in Yellowstone panels (e) and (f) owing to its disparate age and isotopic composition relative to other Heise units (see text for more detail).

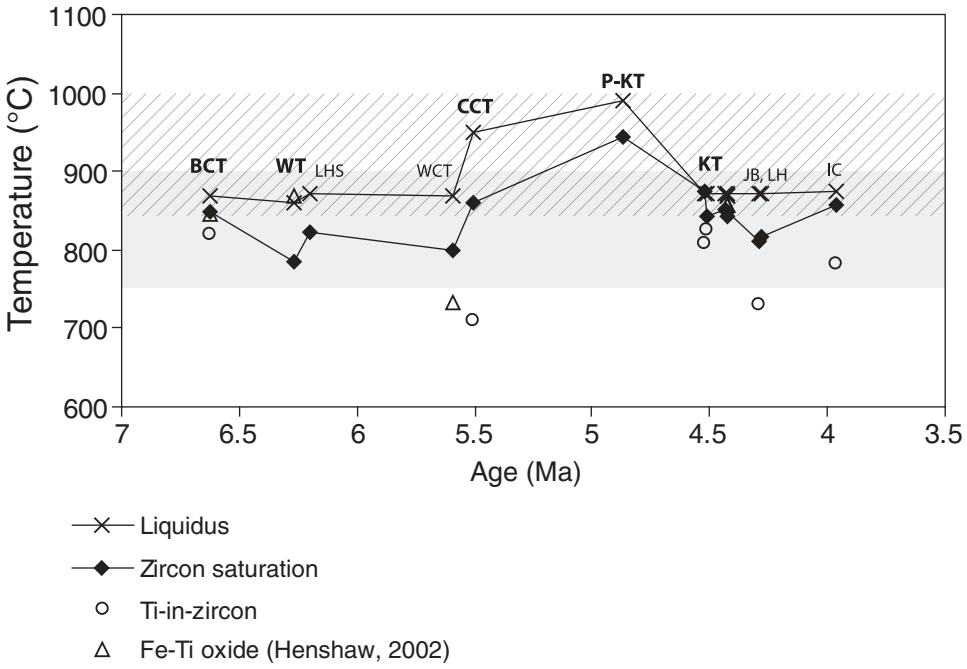

Fig. 12. Magmatic temperatures of Heise rhyolites as determined by several independent methods (MELTS liquidus temperatures, zircon saturation temperatures, and Ti-in-zircon temperatures). Fe–Ti oxide temperatures from Henshaw (2002) are also included. Labels for Heise units correspond to those used in Fig. 5. Most Heise rhyolites had magmatic temperatures of ~800–900°C. The Pre-Kilgore Tuff (P-KT) had the highest magmatic temperature of ~950–1000°C. Magmatic temperature ranges for Yellowstone rhyolites (gray field) and Bruneau–Jarbidge rhyolites (diagonally shaded field) are shown for comparison.

crustal depth) and rapid (tens to hundreds of thousands of years) generation of the largest-known low-$\delta^{18}O$ rhyolite in the world is correct, then it provides a compelling case for the occurrence of similar processes worldwide, which may or may not fingerprint eruptive products with the tell-tale low-$\delta^{18}O$ signatures. Our results would seemingly falsify conventional wisdom of slow magma genesis in the deeper crust and call for thermo-mechanical models to answer these questions.

Normal-$\delta^{18}O$ magma genesis in the Heise volcanic field

Rhyolitic volcanism in the Heise volcanic field began at 6·62 Ma with the 1200 km^3 caldera-forming eruption of the normal-$\delta^{18}O$ Blacktail Creek Tuff, which has a SiO_2–$\delta^{18}O$ composition that overlaps that of SRP continental crust (Fig. 10a and b) and a whole-rock normative composition that corresponds to the low-pressure (1–2 kbar) granite minimum in the Ab–Or–Qtz system (Fig. 5). It has the most radiogenic Sr isotope signature of all Heise units (Fig. 11c), indicating that it has the strongest affinity to SRP Archean crust. Its genesis can be explained by ~35% partial melting of SRP Archean crust, based on its near-eutectic granitic composition (Fig. 5) and trace element enrichments and depletions relative to the average upper continental crust composition of Taylor & McLennan (1985) and McLennan *et al.* (2006) (Appendix C). Subsequent normal-$\delta^{18}O$ caldera-forming eruptions of the 750 km^3 Walcott Tuff at 6·27 Ma and the 300 km^3 Conant Creek Tuff at 5·51 Ma were ~0·5–0·7‰ lower in $\delta^{18}O$ than the Blacktail Creek Tuff, but still within the normal-$\delta^{18}O$ range for high-silica rhyolites (Figs 7b and 10a, b). These rhyolites maintain the same basic mineralogy (± quartz), mineral chemistry, and whole-rock major element geochemistry as the Blacktail Creek Tuff (Tables 1–3), but define a divergent temporal compositional trend in trace element concentrations of Ba, Y, Nb, La, Ce and Nd (Table 3), Rb/Sr, Rb/Ba, Zr/Nb, La/Nb and Ce/Nb trace element ratios (Fig. 6a–e), and $^{87}Sr/^{86}Sr$ and $^{143}Nd/^{144}Nd$ ratios (Fig. 11c and d).

The data support derivation of the normal-$\delta^{18}O$ Blacktail Creek Tuff, Conant Creek Tuff and Walcott Tuff from a common rhyolitic magma source that was assembled from large-degree (~35%) partial melts of normal-$\delta^{18}O$ SRP crust (Appendix C). Fractional crystallization of ~10–15%, involving plagioclase, clinopyroxene and zircon, of such a magma source can explain the variations in trace element concentrations in these successive caldera-forming eruptions (Appendix B). Because there were 350–760 kyr time gaps between successive eruptions, we do not envision a continuous liquid line of descent from a single magma reservoir, but rather a scenario in

which the residual magma was periodically cooled below the solidus and reactivated by fresh injections of basalt, yielding large-volume normal-$\delta^{18}O$ tuffs over the course of ~1 Myr that retain evidence of a common lineage. We do not attempt to determine whether the reservoir remained in a mushy state (Bachmann & Bergantz, 2004) or was produced by periodic underplating by SRP basalt (Leeman *et al.*, 2008; McCurry & Rodgers, 2009). However, the high magmatic temperatures of the Heise rhyolites contradict derivation from a near-solidus mush, which would be expected to have temperatures less than 800°C. The progressive decrease in $^{87}Sr/^{86}Sr$ and increase in $^{143}Nd/^{144}Nd$ in normal-$\delta^{18}O$ Heise tuffs may be due to a greater basalt versus crust contribution through time, as periodic injections of basalt accrued in the normal-$\delta^{18}O$ crustal block.

Low-$\delta^{18}O$ Kilgore Tuff magma genesis

Origin of the low-$\delta^{18}O$ signature of the Kilgore Tuff

The low-$\delta^{18}O$ magmatic values (3·2–3·6‰) of the voluminous Kilgore Tuff require that a significant proportion of its oxygen was derived from low-$\delta^{18}O$ meteoric waters (e.g. Friedman *et al.*, 1974; Hildreth *et al.*, 1984; Taylor, 1986). Direct exchange with meteoric water diffusing into the melt is an unrealistic scenario given the slow rate of water diffusion into silicic melts and the large amounts of dissolved water (tens of per cent) required to generate O isotope depletions of this magnitude (e.g. Taylor, 1986). Syneruptive exchange between magmas and low-$\delta^{18}O$ crust (e.g. Garcia *et al.*, 1998) is also unlikely owing to the $\delta^{18}O$ homogeneity of the Kilgore Tuff and the fact that it contains tuff and sandstone lithic fragments that are normal–high-$\delta^{18}O$ (Fig. 3). The possibility of a low-$\delta^{18}O$ source, such as the Idaho Batholith (e.g. Boroughs *et al.*, 2005), is not likely given the fact that all crustal xenoliths and basalts analyzed in the eastern SRP have normal-$\delta^{18}O$ signatures (Hildreth *et al.*, 1984; Watts *et al.*, 2010). The time-progressive depletion in $\delta^{18}O$ (Fig. 7b) indicates that a process fundamental to the evolution of the Heise volcanic field is key to the genesis of the large-volume low-$\delta^{18}O$ Kilgore Tuff.

Correlation between cumulative eruptive volumes and low-$\delta^{18}O$ signatures

Oxygen is the most abundant element in the Earth's crust and mantle, and thus it is useful to consider the correlation between cumulative eruptive volumes and magmatic $\delta^{18}O$ signatures when assessing rhyolite genesis from crustal and mantle sources. A linear least-squares regression line fit to 16 Heise units for $\delta^{18}O$ versus cumulative eruptive volume demonstrates a strong negative correlation between the two parameters, with an $R^2 = 0{\cdot}86$ (Fig. 13a). We assume that (1) the erupted rhyolite volumes correspond to similar erupted/intrusive proportions for each tuff, and (2) the magnitude and direction of error in the volume estimates is comparable. Operating under these assumptions, the equation of the line of best fit can be used to predict $\delta^{18}O$ values for a given cumulative eruptive volume. Increments of 1000 km^3 decrease the $\delta^{18}O$ value by ~1‰, with cumulative eruptive volumes of 1000 km^3, 2000 km^3, 3000 km^3, and 4000 km^3 corresponding to $\delta^{18}O$ values of *c.* 7‰, 6‰, 5‰, and 3–4‰, respectively (Fig. 13a and c).

The data support a systematic progression of shallow crustal recycling in Heise rhyolite genesis, whereby progressively larger proportions of shallow, hydrothermally altered (low-$\delta^{18}O$) crust are tapped in successive rhyolite eruptions. High-temperature oxygen isotope exchange between normal-$\delta^{18}O$ rocks (>6‰) and low-$\delta^{18}O$ Heise meteoric waters (<−10‰) creates hydrothermally altered low-$\delta^{18}O$ rock reservoirs, which upon remelting yield low-$\delta^{18}O$ magmas. Caldera-forming eruptions facilitate this process; pervasive fracturing of the crust during caldera collapse generates conduits for meteoric fluid flow, and thus the development of a hydrothermal system, and vertical downdrop of the caldera floor brings hydrothermally altered intracaldera and subcaldera rocks closer to the underlying heat source for remelting (e.g. Bindeman & Valley, 2001; Bindeman *et al.*, 2007). This effect is amplified in a nested caldera environment, as it results in maximum fracturing and vertical drawdown. Low-$\delta^{18}O$ Kilgore cycle magmas ($\delta^{18}O$ of ~3–4‰), which erupted after three overlapping caldera collapses and ~2000 km^3 of erupted rhyolite, signify the terminal stage of rhyolite genesis from the crustal block. Below, we compare the Heise trend with the trends observed for the Yellowstone and Bruneau–Jarbidge rhyolites.

Like that observed for Heise, a trend of decreasing $\delta^{18}O$ with cumulative eruptive volume is evident for the Yellowstone rhyolite units (Fig. 13a). A linear least-squares regression line fit to 17 Yellowstone units yields a nearly identical equation to the one derived for Heise data, though the R^2 value is less robust owing to the greater spread in Yellowstone $\delta^{18}O$ data (Fig. 13a). Greater spread in the Yellowstone data is attributed to Pleistocene glaciations that generated significant (negative) torque on the oxygen isotopic values of Yellowstone magmas (Hildreth *et al.*, 1984). In contrast, the isotopic compositions of the Miocene–Pliocene Heise magmas were probably not affected by glaciations. Post-Lava Creek Tuff Central Plateau Member units have $\delta^{18}O$ values that overlap those of the Kilgore Tuff and post-Kilgore units ($\delta^{18}O$ of ~3–4‰) for essentially the same cumulative eruptive volumes (4470 km^3 for Yellowstone versus 4200 km^3 for Heise), providing evidence that they represent a terminal stage of rhyolite generation analogous to the final Kilgore cycle of the Heise volcanic field (Fig. 13a and c).

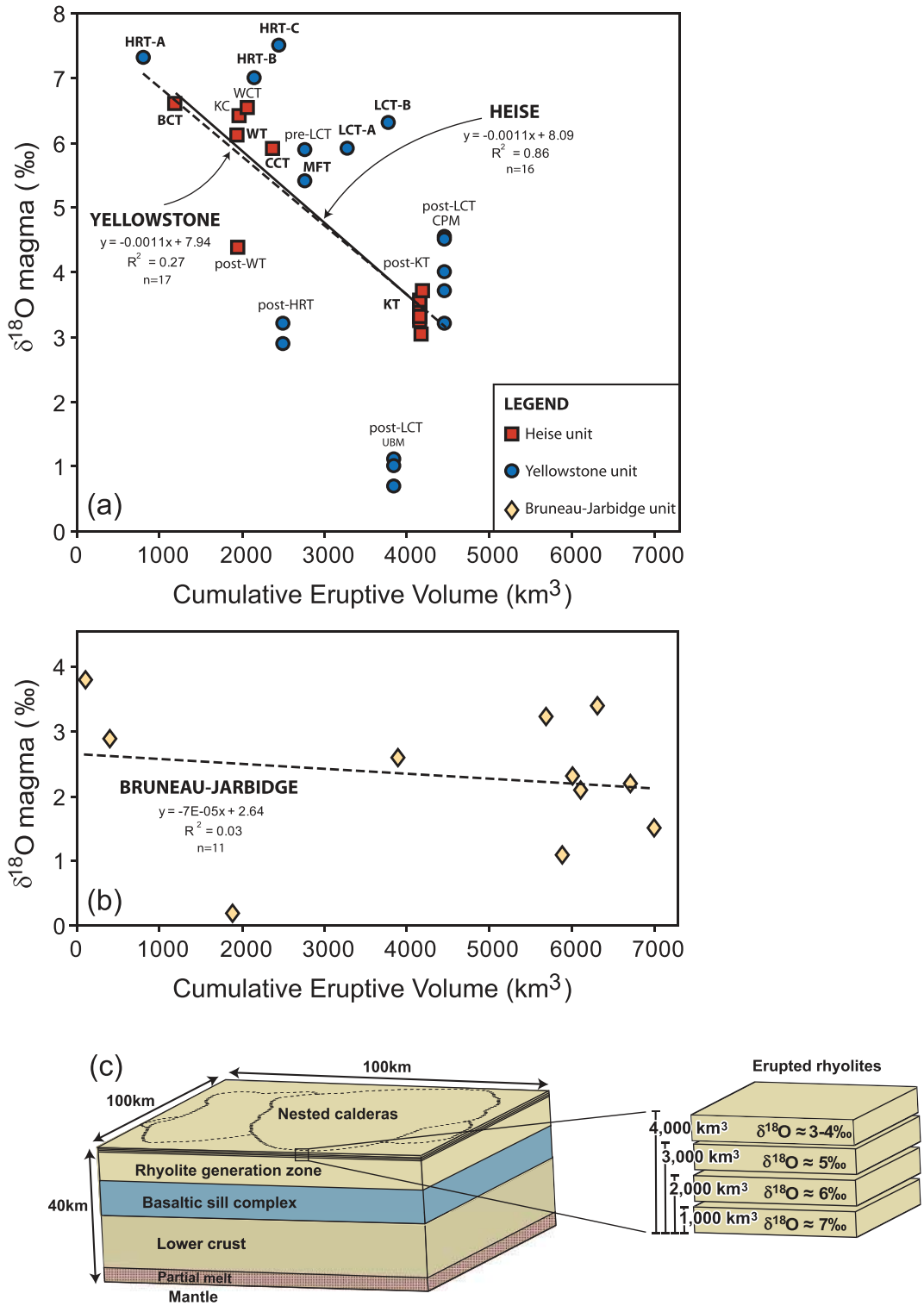

Fig. 13. Magmatic $\delta^{18}O$ vs cumulative eruptive volume. (a) Linear least-squares regression lines for Heise (continuous line; $n = 16$) and Yellowstone (dashed line; $n = 17$) rhyolites show a trend of decreasing $\delta^{18}O$ with cumulative eruptive volume. Magmatic $\delta^{18}O$ values and eruptive volumes for the Heise units are shown in Table 1. Data for Yellowstone units are synthesized from Hildreth *et al.* (1984), Bindeman & Valley (2001), Christiansen (2001), Christiansen *et al.* (2007) and Bindeman *et al.* (2008) (see Supplementary Data Table 4). (b) A linear least-squares regression line for Bruneau–Jarbidge (dashed line) rhyolites shows no trend between $\delta^{18}O$ and cumulative eruptive volume. Magmatic $\delta^{18}O$ values and eruptive volumes for Bruneau–Jarbidge units are synthesized from Bonnichsen *et al.* (2008), Leeman *et al.* (2008), and B. Ellis (unpublished) (see Supplementary Data Table 4). (c) Schematic depiction of the crustal block in the eastern Snake River Plain (after Peng & Humphreys, 1998) showing the Heise–Yellowstone trend of decreasing magmatic $\delta^{18}O$ with cumulative eruptive volume. Magmatic $\delta^{18}O$ values are lowered by ~1‰ for every 1000 km^3 of erupted rhyolite.

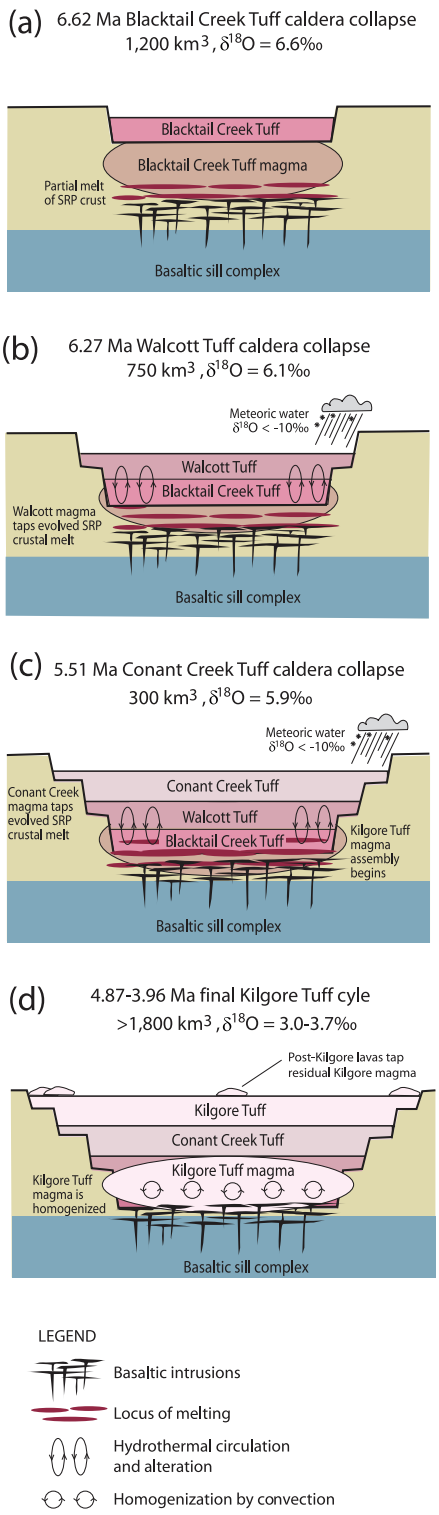

Fig. 14. Schematic model of rhyolite genesis in the Heise volcanic field. (a) Blacktail Creek Tuff magma assembles from partial melts of normal-$\delta^{18}O$ Snake River Plain (SRP) crust induced by heating from basaltic intrusions in an underlying sill complex [seismically imaged by Peng & Humphreys (1998)]. Blacktail Creek Tuff caldera collapse accommodates the intracaldera fill. (b) Walcott Tuff magma taps evolved, normal-$\delta^{18}O$ SRP crustal melts. Walcott Tuff caldera collapse spatially overlaps the Blacktail Creek Tuff caldera, forming a nested caldera complex that brings intracaldera fill material closer to the underlying heat source. Meteoric waters penetrate shallow caldera fractures, leading to hydrothermal alteration of intracaldera fill by circulating fluids. (c) Conant Creek Tuff magma taps further evolved, normal-$\delta^{18}O$ SRP crustal melts. The slightly low-$\delta^{18}O$ signature of the Conant Creek Tuff magma (~0·1‰ depleted relative to normal-$\delta^{18}O$ rhyolites) can be explained by a minor contribution from hydrothermally altered (low-$\delta^{18}O$) materials. Conant Creek Tuff caldera collapse spatially overlaps the Blacktail Creek and Walcott calderas, resulting in maximum vertical drawdown of the intracaldera rocks. Assembly of the Kilgore Tuff magma begins when hydrothermally altered (low-$\delta^{18}O$) Blacktail Creek Tuff intracaldera rocks intercept the locus of melting above the basaltic sill complex. (d) Kilgore Tuff magma is homogenized as melt pockets coalesce on a large scale to form a voluminous low-$\delta^{18}O$ magma body, ~3‰ depleted relative to the normal-$\delta^{18}O$ rhyolites. Post-Kilgore lavas tap residual low-$\delta^{18}O$ Kilgore Tuff magma, and erupt along the ring fracture zone and as domes in the center of the Kilgore caldera.

Bruneau–Jarbidge units do not reveal a trend of decreasing $\delta^{18}O$ with cumulative eruptive volume, as observed for the younger and better exposed Heise and Yellowstone units (Fig. 13b). One obvious explanation for the lack of a trend in the Bruneau–Jarbidge units is that eruptive volumes, unit designations, and correlations are poorly defined as a result of erosion and burial by younger units (Bonnichsen *et al.*, 2008). Because eruptions in the Bruneau–Jarbidge volcanic field are exclusively low-$\delta^{18}O$ ($\delta^{18}O$ of ~0–4‰), it may be most instructive to compare them with the final stage of low-$\delta^{18}O$ eruptions at Heise (Kilgore Tuff and post-Kilgore units) and Yellowstone (post-Lava Creek Tuff units). For instance, if eruptions were to continue at Heise and Yellowstone beyond 4200 km^3 and 4470 km^3, it is conceivable that the linear trends would flatten at some critical stage of $\delta^{18}O$ depletion, owing to the limitations of oxygen isotope exchange in shallow crustal conditions (e.g. Taylor, 1986). It may be that the extremely low-$\delta^{18}O$ values of the majority of Bruneau–Jarbidge rhyolites ($\delta^{18}O$ of ~0–3‰) represent this critical threshold. We do not exclude the possibility that normal-$\delta^{18}O$ eruptions, like the Jarbidge rhyolite (see 'Oxygen isotopes' section), preceded the low-$\delta^{18}O$ Bruneau–Jarbidge eruptions. The presence of normal-$\delta^{18}O$ zircons in low-$\delta^{18}O$ Cougar Point Tuff units (Cathey *et al.*, 2008) may be indicative of such a scenario.

The Blacktail Creek Tuff: Source of the low-$\delta^{18}O$ Kilgore Tuff

Based on the new evidence presented in this work, we suggest that the Kilgore Tuff was derived from remelting hydrothermally altered (low-$\delta^{18}O$) volcanic and intrusive portions of the massive Blacktail Creek Tuff, which would have been the deepest, and thus closest to the underlying basaltic heat source, after three prior overlapping

caldera-forming eruptions (Fig. 14a–d). This would allow the Kilgore Tuff to maintain the same basic mineralogy (Table 2), mineral chemistry (Table 2), normative composition and phase relations (Fig. 5) as the Blacktail Creek Tuff, but possess a lower $\delta^{18}O$ signature owing to the ^{18}O depletion of the Blacktail Creek Tuff protolith. Our observation that the final low-$\delta^{18}O$ Kilgore Tuff cycle magmas define a reversal from the evolutionary trend of earlier tuff eruptions (Blacktail Creek, Walcott, Conant Creek) back towards the Blacktail Creek Tuff composition in trace element concentrations of Ba, Y, Nb, La, Ce and Nd, trace element ratios of Rb/Sr, Rb/Ba, Zr/Nb, La/Nb and Ce/Nb, and $^{87}Sr/^{86}Sr$ and $^{143}Nd/^{144}Nd$ isotope ratios, supports this hypothesis (Figs 6a–e and 11c, d). Further supporting evidence is the presence of twinned clinopyroxene crystals, which are observed only in samples of the Blacktail Creek Tuff and Kilgore Tuff (Fig. 4g and h), and the presence of normal-$\delta^{18}O$ tuff lithic fragments within a low-$\delta^{18}O$ Kilgore Tuff vitrophyre (Fig. 3) that match the $\delta^{18}O$ composition of the Blacktail Creek Tuff ($\delta^{18}O \approx 7‰$) (Fig. 7b).

Assuming a 1·5 kJ kg^{-1} K^{-1} heat capacity for basalt (Snyder, 2000), 750°C cooling of basalt from ~1250°C liquidus to 500°C ambient temperature, and a 400 kJ kg^{-1} latent heat of crystallization (Grunder, 1995), the heat contribution to the shallow crust from basalt is estimated to be *c.* 1500 kJ kg^{-1}. The heat required to melt glassy, high-silica rhyolite would be *c.* 500 kJ kg^{-1}, based on a 1·3 kJ kg^{-1} K^{-1} heat capacity of rhyolite (Snyder, 2000), 350°C heating of rhyolite from 500°C ambient temperature to 850°C liquidus, and negligible latent heat of fusion. With a basalt heat transfer efficiency of 20–40% (Dufek & Bergantz, 2005), a basalt volume of ~1–2 times the volume of rhyolite is required. Thus, at high (e.g. Hawaiian) basalt production rates of 0·01 km^3 a^{-1}, *c.* 100–300 kyr would be necessary to generate the voluminous 1800 km^3 Kilgore Tuff by remelting intracaldera portions of the Blacktail Creek Tuff.

Achieving homogeneity in the Kilgore Tuff

Homogeneity in $\delta^{18}O$ values, $^{87}Sr/^{86}Sr$ and $^{143}Nd/^{144}Nd$ ratios, liquidus temperatures and U–Pb zircon ages of samples erupted >100 km apart indicates that the Kilgore Tuff was derived from an extremely voluminous, homogeneous magma chamber. Rather than remelting of an isotopically homogeneous reservoir of low-$\delta^{18}O$ source rocks, it is much more likely that the Kilgore Tuff was incrementally assembled from isotopically heterogeneous batches of melt, generated from remelting of isotopically heterogeneous source rocks altered by variable water–rock ratios. Ion probe oxygen isotope analyses of single Kilgore Tuff zircons, which are heterogeneous within a low-$\delta^{18}O$ range of *c.* −1 to 3‰ (Fig. 8), support this interpretation. We envision a large subcaldera magma source region (probably >6000 km^2 based on the footprint of the Kilgore caldera), in which the primary isotopic heterogeneities of the original protoliths, and secondary heterogeneities resulting from their subsequent alteration, were averaged on a caldera-wide scale. Batches of heterogeneous melt aggregated to form a single well-mixed convecting magma body with a homogeneous geochemical and isotopic composition (Fig. 14c and d). Only refractory zircon phenocrysts retain evidence of this batch assembly process, whereas the less refractory phenocryst phases and host glass were completely reset. Given the fact that the U–Pb ages of single zircons with variable $\delta^{18}O$ values all overlap within an ~300–400 kyr error (Fig. 8), this batch assembly process occurred relatively rapidly.

The Pre-Kilgore Tuff and Post-Kilgore rhyolites

The Pre-Kilgore Tuff is tens to hundreds of thousands of years older than the Kilgore Tuff, as indicated by multiple stratigraphic time breaks within ~11 m of section that separate it from the Kilgore Tuff (Fig. 3) and its U–Pb zircon crystallization age of 4·87 Ma (versus 4·58 Ma for the Kilgore Tuff). However, the Pre-Kilgore Tuff has a magmatic $\delta^{18}O$ signature (3·5‰) that is identical to that of the low-$\delta^{18}O$ Kilgore Tuff cycle, and all analyzed phenocryst phases in the Pre-Kilgore Tuff are within the $\delta^{18}O$ range of Kilgore Tuff phenocrysts (Figs 7b and 8), indicating that it is probably a genetically related precursor of the Kilgore Tuff. Sr isotope ratios provide additional evidence for this genetic link (Fig. 11c), and although the $^{143}Nd/^{144}Nd$ ratio of the Pre-Kilgore Tuff is lower than that of the Kilgore Tuff (Fig. 11d), variations of the observed magnitude are not uncommon for different members of large tuff units (see Hildreth *et al.*, 1991; Fig. 11f). The magmatic temperature of the Pre-Kilgore Tuff (~950–1000°C) was ~100°C higher than the other Heise rhyolites, and may represent a hot, initial phase of Kilgore Tuff genesis in which low-$\delta^{18}O$ melt pockets were beginning to accrete on a large scale.

Post-Kilgore rhyolites have U–Pb zircon crystallization ages that overlap those of the Kilgore Tuff and low-$\delta^{18}O$ oxygen isotope signatures between 3·0 and 3·7‰ that are identical to those of the Kilgore Tuff (Table 1; Fig. 7b), indicating that they were probably derived from residual low-$\delta^{18}O$ Kilgore Tuff magma (Fig. 14d). Additional evidence of their common heritage includes their more evolved major element compositions (Table 3), similar Ab–Or–Qtz normative compositions (Fig. 5), similar concentrations of trace elements (Table 3), nearly identical $^{87}Sr/^{86}Sr$ and $^{143}Nd/^{144}Nd$ ratios (Fig. 11c and d), and common liquidus temperatures of ~850–870°C (Table 1). We also observe that all Kilgore and post-Kilgore samples contain glomerocrystic clusters of plagioclase, orthopyroxene and clinopyroxene (Fig. 4c–f), which are absent in other Heise units. U–Pb zircon dating of the 3·96 Ma Indian Creek rhyolite shows that it has inherited zircon cores that are the same age as the

Kilgore Tuff (4·46 Ma), establishing a possible genetic link between them (Table 1). About 10% fractional crystallization of the less evolved Pre-Kilgore Tuff magma reservoir would have been required to generate the more evolved Kilgore Tuff and post-Kilgore rhyolites (Appendix B).

Systematic pattern of low-$\delta^{18}O$ rhyolite genesis at Heise, Yellowstone and Bruneau–Jarbidge

Key similarities exist between the Heise, Yellowstone Plateau and Bruneau–Jarbidge volcanic fields, and the Kilgore Tuff serves as an important bridging link between them. When looking at trends in magmatic $\delta^{18}O$ through time, a few striking features are apparent in all three volcanic fields: (1) after the first 1–2 caldera collapse events the oxygen isotope trend plunges sharply by ~3–4‰; (2) over the next ~1 Myr of caldera-forming eruptions the oxygen isotope signatures rebound by ~2–3‰; (3) in the final pulse of volcanism the ~2–3‰ recovery is reversed and the low-$\delta^{18}O$ signature re-emerges (Fig. 7a–c). The Kilgore Tuff of the Heise volcanic field is an explosive low-$\delta^{18}O$ tuff, like the Cougar Point tuffs in the Bruneau–Jarbidge volcanic field, but it was erupted after a series of normal-$\delta^{18}O$ tuffs, like the low-$\delta^{18}O$ rhyolite lavas of the Yellowstone Plateau volcanic field. The magnitude and timing of the $\delta^{18}O$ depletions are comparable in all three volcanic fields, but the oscillations are within a ~0–4‰ range at Bruneau–Jarbidge, a ~3–7‰ range at Heise and a ~0–8‰ range at Yellowstone (Fig. 7a–c).

In addition to a progressive transition in O isotope compositions, a transition in Sr and Nd isotope compositions is also apparent in the three volcanic fields. Heterogeneity in Sr and Nd isotope ratios increases from west to east (Fig. 11a–f), probably as a result of changes in the composition of the crust, from thinner and less radiogenic crust in the central SRP to thicker, more radiogenic and more refractory crust in the eastern SRP (see Leeman *et al.*, 1992; Manduca *et al.*, 1992; Nash *et al.*, 2006). Consequently, the nature (e.g. depth, magnitude, frequency) of large silicic caldera-forming eruptions, and in turn, the style of low-$\delta^{18}O$ rhyolite genesis, varies in a systematic way. Thinner, less refractory crust provides a significant thermal advantage over thick, refractory crust in the formation of shallow crustal melts by heating induced by mantle-derived basalt (e.g. Manea *et al.*, 2009); consequently, the number of caldera-forming eruptions is higher in regions of thinner crust (Nash *et al.*, 2006; Bonnichsen *et al.*, 2008; Leeman *et al.*, 2008). Frequent, overlapping caldera-forming eruptions promote large-scale fracturing of the crust and the development of a pervasive hydrothermal system early in the lifespan of a volcanic field. Thus, at Bruneau–Jarbidge, low-$\delta^{18}O$ rhyolite genesis may have happened essentially instantaneously owing to the high frequency of hot, spatially overlapping caldera-forming eruptions at the onset of volcanism, whereas at Heise and Yellowstone, preconditioning of the much thicker, more refractory crust over a ~2 Myr period was required before low-$\delta^{18}O$ rhyolites dominated.

The Kilgore Tuff: an analog for Quaternary rhyolite eruptions at Yellowstone

The low-$\delta^{18}O$ Kilgore Tuff has many similarities to the 0·26–0·08 Ma Central Plateau Member rhyolites of the Yellowstone Plateau volcanic field, and thus may serve as their analog. Like the Kilgore Tuff, Central Plateau Member rhyolites erupted after three prior caldera-forming eruptions (~2 Myr after the initiation of volcanism) and are characterized by low $\delta^{18}O$ values that are ~3‰ depleted relative to normal-$\delta^{18}O$ tuffs (Fig. 7a and b). Both the Kilgore Tuff and Central Plateau Member rhyolites are extremely voluminous, ~1800 km^3 and ~620 km^3, respectively, but differ in the fact that the Kilgore Tuff is an explosive caldera-forming tuff and the Central Plateau Member rhyolites are mostly effusive post-caldera lavas. Rhyolites of the Heise and Yellowstone Plateau volcanic fields define a negative correlation between $\delta^{18}O$ values and cumulative eruptive volumes, with the Kilgore Tuff and Central Plateau Member rhyolites corresponding to ~4000–4500 km^3 of erupted rhyolite, and heralding the terminal stages of rhyolite generation in each volcanic field (Fig. 13a).

In our preferred model of low-$\delta^{18}O$ rhyolite genesis, the evolution from normal-$\delta^{18}O$ to low-$\delta^{18}O$ rhyolites is an expected consequence of large-volume silicic magmatism in nested caldera complex settings, in which each successive caldera-forming eruption displaces material from the crustal block and accommodates vertical downdrop of shallow, hydrothermally altered (^{18}O depleted) intracaldera rock for remelting (Fig. 14a–d; Bindeman & Valley, 2001; Bindeman *et al.*, 2007; Watts *et al.*, 2010). Whereas the low-$\delta^{18}O$ Kilgore Tuff was probably produced by batch assembly of pockets of melt from variably hydrothermally altered sources that were homogenized in a single, voluminous magma body, the Central Plateau Member rhyolites represent an intermediate stage of assembly, whereby both small and large pockets of melt erupted effusively prior to coalescing into a single magma chamber beneath the crust.

CONCLUSIONS

The Kilgore Tuff is the largest-known low-$\delta^{18}O$ rhyolite yet discovered. U–Pb zircon ages, mineral chemistry, whole-rock major and trace element geochemistry, Sr and Nd isotope geochemistry, and magmatic temperatures corroborate oxygen isotopic evidence that the Kilgore Tuff erupted from an exceptionally large and homogeneous

magma chamber. Extreme oxygen isotopic diversity of ~7‰ in single zircon crystals signifies batch assembly of variably ^{18}O depleted melts prior to homogenization of the Kilgore Tuff magma on a caldera-wide scale. The data support derivation of the Kilgore Tuff magma by remelting and homogenization of variably hydrothermally altered intracaldera and subvolcanic portions of the Blacktail Creek Tuff, which would have been the deepest part of the subsided caldera fill and thus closest to the underlying heat source after three overlapping caldera collapses. Correlations between magmatic $\delta^{18}O$ signatures, eruption ages, and cumulative eruptive volumes at Heise and Yellowstone can be used to predict the Kilgore Tuff's appearance in the Heise volcanic field, and thus support our view that low-$\delta^{18}O$ rhyolite genesis is an expected outcome of caldera cluster evolution in the SRP. Our work further demonstrates that large volumes (thousands of km^3) of hot, crystal-poor rhyolitic magma can be generated by rapid remelting in the shallow crust. The Kilgore Tuff may be a useful analog for the most recent phase of rhyolitic eruptions at Yellowstone, and perhaps other large-volume rhyolites in nested caldera complexes around the world.

ACKNOWLEDGEMENTS

We thank Lisa Morgan for advice on sampling localities and sample donation, Bill Leeman and Bill Bonnichsen for organizing a field trip to the Magic Reservoir eruptive center, Greg Retallack for helpful discussions on paleosols, Erwan Martin for analyzing paleosol samples for $\Delta^{17}O$, and Rachel Weber for fieldwork assistance. We thank Chris Harris, Kurt Knesel and John Wolff for their constructive reviews of the paper.

FUNDING

This work was supported by NSF grant EAR/CAREER-844772 to I.N.B., NSF grant IF-0732691 to the UCLA SIMS facility, and a USGS Kleinman Grant for Volcano Research to K.E.W.

SUPPLEMENTARY DATA

Supplementary data for this paper are available at *Journal of Petrology* online.

REFERENCES

Bachmann, O. & Bergantz, G. W. (2004). On the origin of crystal-poor rhyolites: extracted from batholithic crystal mushes. *Journal of Petrology* **45**, 1565–1582.

Bacon, C. R. (1983). Eruptive history of mount Mazama and Crater Lake caldera Cascade Range, USA. *Journal of Volcanology and Geothermal Research* **18**, 57–115.

Bindeman, I. N. (2008). Oxygen isotopes in mantle and crustal magmas as revealed by single crystal analysis. In: Putirka, K. D. & Tepley, F. J., III (eds) *Minerals, Inclusions and Volcanic Processes. Mineralogical Society of America and Geochemical Society, Reviews in Mineralogy and Geochemistry* **69**, 445–478.

Bindeman, I. N. & Valley, J. W. (2001). Low-$\delta^{18}O$ rhyolites from Yellowstone: magmatic evolution based on analyses of zircons and individual phenocrysts. *Journal of Petrology* **42**, 1491–1517.

Bindeman, I. N. & Valley, J. W. (2002). Oxygen isotope study of the Long Valley magma system, California: isotope thermometry and convection in large silicic magma bodies. *Contributions to Mineralogy and Petrology* **144**, 185–205.

Bindeman, I. N., Valley, J. W., Wooden, J. L. & Persing, H. M. (2001). Post-caldera volcanism: *in situ* measurement of U–Pb age and oxygen isotope ratio in Pleistocene zircons from Yellowstone caldera. *Earth and Planetary Science Letters* **189**, 197–206.

Bindeman, I. N., Ponomareva, V. V., Bailey, J. C. & Valley, J. W. (2004). Kamchatka Peninsula: a province with high-$\delta^{18}O$ magma sources and large scale $^{18}O/^{16}O$ depletion of the upper crust. *Geochimica et Cosmochimica Acta* **68**, 841–865.

Bindeman, I. N., Schmitt, A. K. & Valley, J. W. (2006). U–Pb zircon geochronology of silicic tuffs from the Timber Mt/Oasis Valley caldera complex, Nevada: rapid generation of large-volume magmas by shallow-level remelting. *Contributions to Mineralogy and Petrology* **152**, 649–665.

Bindeman, I. N., Watts, K. E., Schmitt, A. K., Morgan, L. A. & Shanks, P. W. C. (2007). Voluminous low-$\delta^{18}O$ magmas in the late Miocene Heise volcanic field, Idaho: implications for the fate of Yellowstone hotspot calderas. *Geology* **35**, 1019–1022.

Bindeman, I. N., Fu, B., Kita, N. T. & Valley, J. W. (2008). Origin and evolution of Yellowstone silicic magmatism based on ion microprobe analysis of isotopically zoned zircons. *Journal of Petrology* **49**, 163–193.

Bonnichsen, B., Leeman, W. P., Honjo, N., McIntosh, W. C. & Godchaux, M. M. (2008). Miocene silicic volcanism in southwestern Idaho: geochronology, geochemistry, and evolution of the central Snake River Plain. *Bulletin of Volcanology* **70**, 315–342.

Boroughs, S. B., Wolff, J., Bonnichsen, B., Godchaux, M. & Larson, P. (2005). Large volume, low-$\delta^{18}O$ rhyolites of the central Snake River Plain, Idaho, USA. *Geology* **33**, 821–824.

Bowen, G. J., Ehleringer, J. R., Chesson, L. A., Stange, E. & Cerling, T. E. (2007). Stable isotope ratios of tap water in the contiguous United States. *Water Resources Research* **43**, W03419.

Branney, M. J., Bonnichsen, B., Andrews, G. D. M., Ellis, B., Barry, T. L. & McCurry, M. (2008). 'Snake River (SR)-type' volcanism at the Yellowstone hotspot track: distinctive products from unusual, high-temperature silicic super-eruptions. *Bulletin of Volcanology* **70**, 293–314.

Cathey, H. E. & Nash, B. P. (2004). The Cougar Point Tuff: implications for thermochemical zonation and longevity of high-temperature, large-volume silicic magmas of the Miocene Yellowstone hotspot. *Journal of Petrology* **45**, 27–58.

Cathey, H. E. & Nash, B. P. (2009). Pyroxene thermometry of rhyolite lavas of the Bruneau–Jarbidge eruptive center, Central Snake River Plain. *Journal of Volcanology and Geothermal Research* **188**, 173–185.

Cathey, H. E., Nash, B. P., Allen, C. M., Campbell, I. H., Valley, J. W. & Kita, N. (2008). U–Pb zircon geochronology and Ti-in-zircon thermometry of large-volume low-$\delta^{18}O$ magmas of the Miocene Yellowstone hotspot (Goldschmidt conference abstract). *Geochimica et Cosmochimica Acta* **72**, A143.

Charlier, B. L. A., Wilson, C. J. N., Lowenstern, J. B., Blake, S., Van Calsteren, P. W. & Davidson, J. P. (2005). Magma generation at a large hyperactive silicic volcano (Taupo, New Zealand) revealed

by U–Th and U–Pb systematics in zircons. *Journal of Petrology* **46**, 3–32.

Christiansen, R. L. (2001). *The Quaternary and Pliocene Yellowstone Plateau Volcanic Field of Wyoming, Idaho, and Montana. US Geological Survey, Professional Papers* **729-G**, , 145 p.

Christiansen, R. L., Lowenstern, J. B., Smith, R. B., Heasler, H., Morgan, L. A., Nathansen, M., Mastin, L.G., Muffler, L. J. P & Robinson, J. E. (2007). *Preliminary assessment of volcanic and hydrothermal hazards in Yellowstone National Park and vicinity. US Geological Survey Open-File Report* **1071**, , 94 p.

Coats, R. R., Green, R. C., Cress, L. D. & Marks, L. Y. (1977). *Mineral resources of the Jarbidge Wilderness and adjacent areas, Elko County, Nevada. US Geological Survey Bulletin* **1439**, , 79 p.

Criss, R. E. & Fleck, R. J. (1987). Petrogenesis, geochronology, and hydrothermal systems in the northern Idaho batholith and adjacent areas based on $^{18}O/^{16}O$, D/H, $^{87}Sr/^{86}Sr$, K–Ar, and $^{40}Ar/^{39}Ar$ studies. *US Geological Survey Professional Paper* **1436**, 95–137.

Davis, O. K. & Ellis, B. (2010). Early occurrence of sagebrush steppe, Miocene (12 Ma) on the Snake River Plain. *Review of Palaeobotany and Palynology* **160**, 172–180.

Dufek, J. & Bergantz, G. W. (2005). Lower crustal magma genesis and preservation: A stochastic framework for the evaluation of basalt-crust interaction. *Journal of Petrology* **46**, 2167–2195.

Friedman, I., Lipman, P. W., Obradovich, J. D., Gleason, J. D. & Christiansen, R. L. (1974). Meteoric water in magmas. *Science* **184**, 1069–1072.

Fu, B., Page, F. Z., Cavosie, A. J., Fournelle, J., Kita, N. T., Lackey, J. S., Wilde, S. A. & Valley, J. W. (2008). Ti-in-zircon thermometry: applications and limitations. *Contributions to Mineralogy and Petrology* **156**, 197–215.

Gansecki, C. A. (1998). $^{40}Ar/^{39}Ar$ geochronology and pre-eruptive geochemistry of the Yellowstone Plateau volcanic field rhyolites, PhD thesis, Stanford University, Stanford, CA, 213 pp.

Garcia, M. O., Ito, E., Eiler, J. M. & Pietruszka, A. J. (1998). Crustal contamination of Kilauea Volcano magmas revealed by oxygen isotope analyses of glass and olivine from Pu'u O'o eruption lavas. *Journal of Petrology* **39**, 803–817.

Ghiorso, M. S. & Sack, R. O. (1991). Fe–Ti oxide geothermometry: thermodynamic formulation and the estimation of intensive variables in silicic magmas. *Contributions to Mineralogy and Petrology* **108**, 485–510.

Ghiorso, M. S. & Sack, R. O. (1995). Chemical mass-transfer in magmatic processes IV: A revised and internally-consistent thermodynamic model for the interpolation and extrapolation of liquid–solid equilibria in magmatic systems at elevated temperatures and pressures. *Contributions to Mineralogy and Petrology* **119**, 197–212.

Grunder, A. L. (1995). Material and thermal roles of basalt in crustal magmatism: Case study from eastern Nevada. *Geology* **23**, 952–956.

Hackett, W. R. & Morgan, L. A. (1988). Explosive basaltic and rhyolitic volcanism of the eastern Snake River Plain, Idaho. In: Link, P. K. & Hackett, W. R. (eds) *Guidebook to the geology of central and southern Idaho. Idaho Geological Survey Bulletin* **27**, 283–301.

Halliday, A. N., Mahood, G. A., Holden, P., Metz, J. M., Dempster, T. J. & Davidson, J. P. (1989). Evidence for long residence times of rhyolitic magma in the Long Valley magmatic system: the isotopic record in precaldera lavas of Glass Mountain. *Earth and Planetary Science Letters* **94**, 274–290.

Harris, C., Smith, H. S. & le Roex, A. P. (2000). Oxygen isotope composition of phenocrysts from Tristan da Cunha and Gough Island lavas: Variation with fractional crystallization and evidence for assimilation. *Contributions to Mineralogy and Petrology* **138**, 164–175.

Henshaw, N. D. (2002). Temperature of silicic magmas from the Yellowstone hotspot, MS thesis, University of Utah, Salt Lake City, UT, 181 pp.

Hildreth, W. & Wilson, C. J. N. (2007). Compositional zoning of the Bishop Tuff. *Journal of Petrology* **48**, 951–999.

Hildreth, W., Christiansen, R. L. & O'Neil, J. R. (1984). Catastrophic isotopic modification of rhyolitic magma at times of caldera subsidence, Yellowstone Plateau Volcanic Field. *Journal of Geophysical Research* **89**, 8339–8369.

Hildreth, W., Halliday, A. N. & Christiansen, R. L. (1991). Isotopic and chemical evidence concerning the genesis and contamination of basaltic and rhyolitic magmas beneath the Yellowstone Plateau Volcanic Field. *Journal of Petrology* **32**, 63–138.

Honjo, N., McElwee, K. R., Duncan, R. A. & Leeman, W. P. (1986). K–Ar ages of volcanic rocks from the Magic Reservoir eruptive center, Snake River Plain, Idaho. *Isochron West* **46**, 15–19.

Kita, N. T., Ushikubo, T., Fu, B. & Valley, J. W. (2009). High precision SIMS oxygen isotope analysis and the effect of sample topography. *Chemical Geology* **264**, 43–57.

Lanphere, M. A., Champion, D. E., Christiansen, R. L., Izett, G. A. & Obradovich, J. D. (2002). Revised ages for tuffs of the Yellowstone Plateau volcanic field: Assignment of the Huckleberry Ridge Tuff to a new geomagnetic polarity event. *Geological Society of America Bulletin* **114**, 559–568.

Leeman, W. P., Menzies, M. A., Matty, D. J. & Embree, G. F. (1985). Strontium, neodymium and lead isotopic compositions of deep crustal xenoliths from the Snake River Plain: Evidence for Archean basement. *Earth and Planetary Science Letters* **75**, 354–368.

Leeman, W. P., Oldow, J. S. & Hart, W. K. (1992). Lithosphere-scale thrusting in the western US Cordillera as constrained by Sr and Nd isotopic transitions in Neogene volcanic rocks. *Geology* **20**, 63–66.

Leeman, W. P., Annen, C. & Dufek, J. (2008). Snake River Plain–Yellowstone silicic volcanism: Implications for magma genesis and magma fluxes. In: Annen, C. & Zellmer, G. F. (eds) *Dynamics of Crustal Magma Transfer, Storage and Differentiation. Geological Society, London, Special Publications* **304**, 235–259.

Manduca, C. A., Silver, L. T. & Taylor, H. P. (1992). $^{87}Sr/^{86}Sr$ and $^{18}O/^{16}O$ isotopic systematics and geochemistry of granitoid plutons across a steeply dipping boundary between contrasting lithospheric blocks in western Idaho. *Contributions to Mineralogy and Petrology* **109**, 355–372.

Manea, V. C., Manea, M., Leeman, W. P. & Schutt, D. L. (2009). The influence of plume head–lithosphere interaction on magmatism associated with the Yellowstone hotspot track. *Journal of Volcanology and Geothermal Research* **188**, 68–85.

Martin, E. & Bindeman, I. (2009). Mass-independent isotopic signatures of volcanic sulfate from three supereruption ash deposits in Lake Tecopa, California. *Earth and Planetary Science Letters* **282**, 102–114.

Mason, B. G., Pyle, D. M. & Oppenheimer, C. (2004). The size and frequency of the largest explosive eruptions on Earth. *Bulletin of Volcanology* **66**, 735–768.

Matsuhisa, Y. (1979). Oxygen isotopic compositions of volcanic rocks from the east Japan island arc and their bearing on petrogenesis. *Journal of Volcanology and Geothermal Research* **5**, 271–296.

McCurry, M. & Rodgers, D. W. (2009). Mass transfer along the Yellowstone hotspot track I: Petrologic constraints on the volume of mantle-derived magma. *Journal of Volcanology and Geothermal Research* **188**, 86–98.

McLennan, S. M., Taylor, S. R. & Hemming, S. R. (2006). Composition, differentiation, and evolution of continental crust: constraints from sedimentary rocks and heat flow. In: Brown, M.

& Rushmer, T. (eds) *Evolution and Differentiation of the Continental Crust*. Cambridge: Cambridge University Press, pp. 92–134.

Morgan, L. A. (1988). Explosive silicic volcanism in the eastern Snake River Plain, PhD thesis, University of Hawaii–Manoa, Honolulu, HI, 191 p.

Morgan, L. A. & McIntosh, W. C. (2005). Timing and development of the Heise volcanic field, Snake River Plain, Idaho, western USA. *Geological Society of America Bulletin* **117**, 288–306.

Nash, B. P., Perkins, M. E., Christensen, J. N., Lee, D. C. & Halliday, A. N. (2006). The Yellowstone hotspot in space and time: Nd and Hf isotopes in silicic magmas. *Earth and Planetary Science Letters* **247**, 143–156.

Obradovich, J. D. (1992). *Geochronology of the Late Cenozoic volcanism of Yellowstone National Park and adjoining areas, Wyoming and Idaho. US Geological Survey, Open-File Report* **92–408**, 1–45.

O'Neil, J. R., Clayton, R. N. & Mayeda, T. K. (1969). Oxygen isotope fractionation in divalent metal carbonates. *Journal of Chemical Physics* **51**, 5547–5558.

Paces, J. B. & Miller, J. D., Jr (1993). Precise U–Pb ages of Duluth Complex and related mafic intrusions, northeastern Minnesota: Geochronological insights to physical, petrogenetic, paleomagnetic, and tectonomagmatic processes associated with the 1·1 Ga Midcontinent Rift System. *Journal of Geophysical Research* **98**, 13997–14013.

Peng, X. & Humphreys, E. D. (1998). Crustal velocity structure across the eastern Snake River Plain and the Yellowstone swell. *Journal of Geophysical Research* **103**, 7171–7186.

Pierce, K. L. & Morgan, L. A. (1992). The track of the Yellowstone hotspot: volcanism, faulting, and uplift. In: Link, P. K., Kuntz, M. A. & Platt, L. B. (eds) *Regional Geology of Eastern Idaho and Western Wyoming. Geological Society of America, Memoirs* **179**, 1–53.

Rampino, M. R. & Self, S. (1992). Volcanic winter and accelerated glaciation following the Toba super-eruption. *Nature* **359**, 50–52.

Reid, M. R. (2003). Timescales of magma transfer and storage in the crust. In: Rudnick, R. L. (ed.) *The Crust. Treatise on Geochemistry, Vol.3*. Amsterdam: Elsevier, pp. 167–193.

Retallack, G. J., Tanaka, S. & Tate, T. (2002). Late Miocene advent of tall grassland paleosols in Oregon. *Palaeogeography, Palaeoclimatology, Palaeoecology* **183**, 329–354.

Schärer, U. (1984). The effect of initial ^{230}Th disequilibrium on young U–Pb ages: the Makalu case Himalaya. *Earth and Planetary Science Letters* **67**, 191–204.

Schmitt, A. K., Grove, M., Harrison, T. M., Lovera, O., Hulen, J. B. & Walters, M. (2003). The Geysers–Cobb mountain magma system, California (Part 1): U–Pb zircon ages of volcanic rocks, conditions of zircon crystallization and magma residence times. *Geochimica et Cosmochimica Acta* **67**, 3423–3442.

Sheppard, S.M. F. & Harris, C. (1985). Hydrogen and oxygen isotope geochemistry of Ascension Island lavas and granites: Variation with crystal crystallization and interaction with sea water. *Contributions to Mineralogy and Petrology* **91**, 74–81.

Simon, J. I. & Reid, M. R. (2005). The pace of rhyolite differentiation and storage in an 'archetypical' silicic magma system, Long Valley, California. *Earth and Planetary Science Letters* **235**, 123–140.

Simon, J. I., Vazquez, J. A., Renne, P. R., Schmitt, A. K., Bacon, C. R. & Reid, M. R. (2009). Accessory mineral U–Th–Pb ages and ^{40}Ar/^{39}Ar eruption chronology, and their bearing on rhyolitic magma evolution in the Pleistocene Coso volcanic field, California. *Contributions to Mineralogy and Petrology* **158**, 421–446.

Smith, R. B. & Braile, L. W. (1994). The Yellowstone hotspot. *Journal of Volcanology and Geothermal Research* **61**, 121–187.

Snyder, D. (2000). Thermal effects of the intrusion of basaltic magma into a more silicic magma chamber and implications for eruption triggering. *Earth and Planetary Science Letters* **175**, 257–273.

Taylor, H. P., Jr (1986). Igneous rocks: II. Isotopic case studies of circumpacific magmatism. In: Valley, J. W., Taylor, H. P., Jr & O'Neil, J. R. (eds) *Stable Isotopes in High Temperature Geological Processes. Mineralogical Society of America, Reviews in Mineralogy* **16**, 273–316.

Taylor, S. R. & McLennan, S. M. (1985). *The Continental Crust: its Composition and Evolution*. Oxford: Blackwell.

Trail, D., Bindeman, I. N., Watson, E. B. & Schmitt, A. K. (2009). Experimental calibration of oxygen isotope fractionation between quartz and zircon. *Geochimica et Cosmochimica Acta* **73**, 7110–7126.

Vazquez, J. A. & Reid, M. R. (2002). Time scales of magma storage and differentiation of voluminous high-silica rhyolites at Yellowstone caldera, Wyoming. *Contributions to Mineralogy and Petrology* **144**, 274–285.

Vazquez, J. A. & Reid, M. R. (2004). Probing the accumulation history of the voluminous Toba magma. *Science* **305**, 991–994.

Vazquez, J. A., Kyriazis, S. F., Reid, M. R., Sehler, R. C. & Ramos, F. C. (2009). Thermochemical evolution of young rhyolites at Yellowstone: Evidence for a cooling but periodically replenished postcaldera magma reservoir. *Journal of Volcanology and Geothermal Research* **188**, 186–196.

Wark, D. A., Hildreth, W., Spear, F. S., Cherniak, D. J. & Watson, E. B. (2007). Pre-eruption recharge of the Bishop magma system. *Geology* **35**, 235–238.

Watson, E. B. & Harrison, T. M. (1983). Zircon saturation revisited: temperature and compositional effects in a variety of crustal magma types. *Earth and Planetary Science Letters* **64**, 295–304.

Watson, E. B. & Harrison, T. M. (2005). Zircon thermometer reveals minimum melting conditions on earliest Earth. *Science* **308**, 841–844.

Watts, K. E., Leeman, W. P., Bindeman, I. N. & Larson, P. B. (2010). Supereruptions of the Snake River Plain: Two-stage derivation of low-δ^{18}O rhyolites from normal-δ^{18}O crust as constrained by Archean xenoliths. *Geology* **38**, 503–506.

Wyllie, P. J., Huang, W. L., Stern, C. R. & Maaloe, S. (1976). Granitic magmas: possible and impossible sources, water contents, and crystallization sequences. *Canadian Journal of Earth Science* **13**, 1007–1019.

Zheng, Y.-F. (1993). Calculation of oxygen isotope fractionation in anhydrous silicate minerals. *Geochimica et Cosmochimica Acta* **57**, 1079–1091.

APPENDIX A

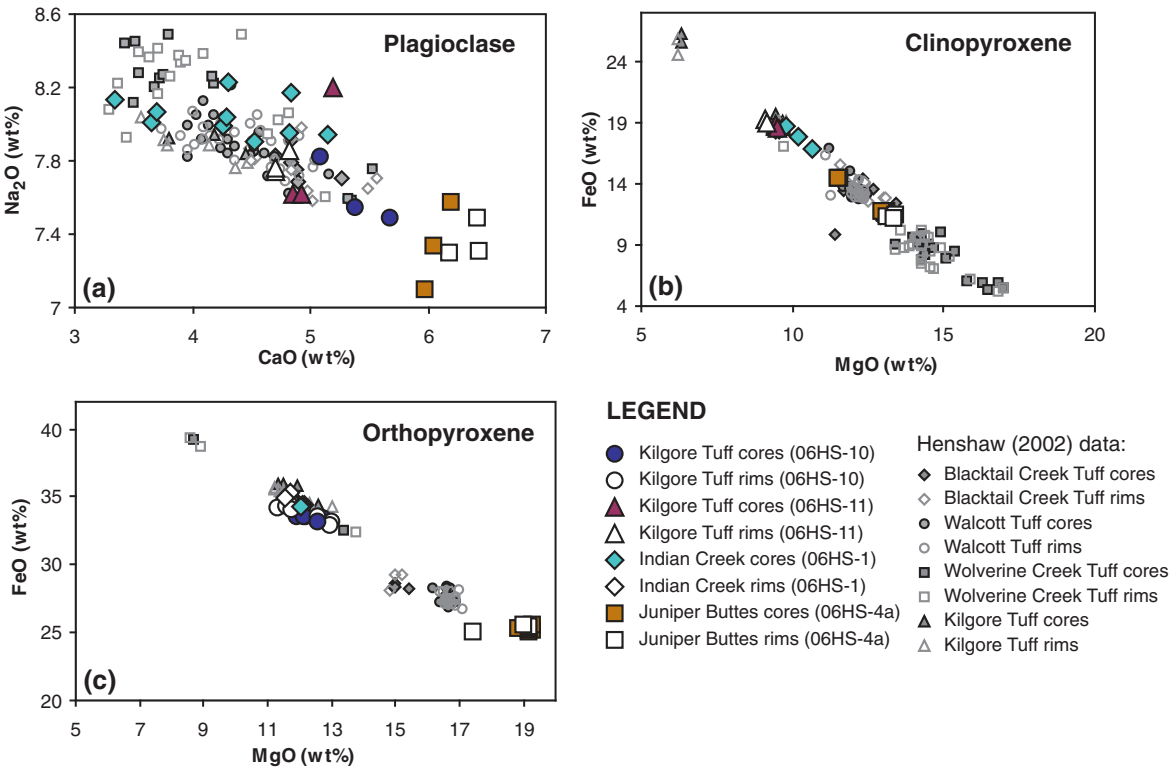

Fig. A1. Compositional variations of Heise phenocrysts. Large symbols are results from this study (see Supplementary Data Table 2); small symbols are results from Henshaw (2002). (a) Na_2O vs CaO in plagioclase showing a wide compositional range and overlap between most Heise units. (b) FeO vs MgO in clinopyroxene showing overlapping compositional fields for Heise units, although some separation is apparent (e.g. Kilgore Tuff). (c) FeO vs MgO in orthopyroxene showing distinct compositional fields for single Heise units.

APPENDIX B: FRACTIONAL CRYSTALLIZATION CALCULATIONS

To estimate the amount of fractional crystallization required to generate the trace element ratio variations observed for successive eruptions of the Blacktail Creek Tuff (BCT), Walcott Tuff (WT) and Conant Creek Tuff (CCT) from a common magma reservoir (see Fig. 6a–e), we used published partition coefficients for Sr, Ba, La and Ce for a high-silica rhyolite composition (earthref.org) and the equation

$$F' = \left(\frac{C_l}{C_o}\right)^{\left[\frac{1}{(\bar{D}-1)}\right]}$$

where F' is the fraction of original liquid remaining, C_o is the trace element concentration in the original liquid, C_l is the trace element concentration in the liquid after crystallization, and $\bar{D}$ is the bulk partition coefficient for a modal mineralogy of 0·8975 plagioclase (plag), 0·10 clinopyroxene (cpx), and 0·0025 zircon, which is consistent with our petrographic observations. Using the same approach, we also estimate the amount of fractional crystallization required to generate the Kilgore Tuff (KT) from the Pre-Kilgore Tuff (P-KT). Our results indicate ~10–15% fractional crystallization ($1 - F'$) steps from the Blacktail Creek Tuff (C_o) to the Walcott Tuff (C_l) and the Walcott Tuff (C_o) to the Conant Creek Tuff (C_l) (see Table A1). We chose Kilgore Tuff samples 06HS-10 and 06HS-11 to estimate the amount of fractional crystallization of the Pre-Kilgore Tuff (06HS-14), as these samples are from the same stratigraphic section as the Pre-Kilgore Tuff (see Fig. 3). The results indicate ~10% fractional crystallization of the Pre-Kilgore Tuff to generate the Kilgore Tuff (see Table B1).

APPENDIX C: CRUSTAL MELTING CALCULATIONS

To estimate the amount of melting required to generate the trace element composition of the earliest Heise Tuff, the Blacktail Creek Tuff (95-2001a), from the upper continental crust composition of Taylor & McLennan (1985) and McLennan *et al.* (2006), we used published partition coefficients for a suite of trace elements for granite compositions (earthref.org) and the modal batch melting equation

$$F = \frac{C_o/(C_l - \bar{D})}{1 - \bar{D}}$$

where F is the melt fraction, C_o is the trace element concentration in the original solid (upper continental crust), C_l is the trace element concentration in the melt (95-2001a), and $\bar{D}$ is the bulk partition coefficient for a modal mineralogy of 0·85 plagioclase (plag), 0·10 clinopyroxene (cpx), 0·4 magnetite (mt), and 0·1 ilmenite (ilm), which is consistent with the modal mineralogy for upper crustal xenoliths in the Snake River Plain (Leeman *et al.*, 1985). The results indicate an average melt fraction of ~36% ± 4% (2 standard error), and thus ~30–40% melting of the upper continental crust would have been required to generate the Blacktail Creek Tuff (see Table C1).

Table B1: Fractional crystallization calculations

	Partition coefficients			$\bar{D}$		BCT–WT	WT–CCT	P-KT–KT	P-KT–KT
	Plag	Cpx	Zircon		C_o:*	95-2001a	06HS-18	06HS-14	06HS-14
					C_l:*	06HS-18	06HS-5	06HS-10	06HS-11
					F'		F'	F'	F'
Sr	6·8	0·98	—	6·20	Sr	0·86	0·91	0·80	0·81
Ba	6·95	0·1	—	6·25	Ba	0·97	0·89	0·98	0·98
La	0·07	0·52	7·2	0·13	La	0·91	0·87	0·92	0·94
Ce	0·032	1·54	10	0·21	Ce	0·85	0·82	1·03	0·99
Modal %	0·8975	0·10	0·0025		Av. F'	0·90	0·87	0·93	0·93
					1 - F'	0·10	0·13	0·07	0·07

*See Table 3 for trace element concentrations for samples 95-2001a, 06HS-18, 06HS-5, 06HS-14, 06HS-10 and 06HS-11.

Table C1: Crustal melting calculations

	Partition coefficients				$\bar{D}$	C_o	C_l	F
	Plag	Cpx	Mt	Ilm		Upper crust*	95-2001a	
Rb	0·06	0·03	0·01	—	0·05	112	174	0·62
Ba	0·19	0·1	0·1	—	0·18	550	1099	0·39
Th	0·11	0·1	0·01	0·427	0·11	10·7	33	0·24
U	0·13	0·12	0·74	0·063	0·15	2·8	7	0·33
Nb	0·07	0·02	—	6·58	0·13	12·0	31·8	0·29
La	0·07	0·52	0·8	1·31	0·16	30	66	0·36
Ce	0·22	0·84	0·71	1·19	0·31	64	120	0·33
Pb	0·5	0·2	0·32	0·34	0·46	17	26	0·35
Sr	6·8	0·98	0·017	0·74	5·89	350	84	0·35
Nd	0·19	1·4	0·93	0·96	0·35	26	45	0·35
Zr	0·36	0·29	0·24	0·49	0·35	190	327	0·36
Y	0·21	0·86	0·12	0·024	0·27	22	44	0·31
Sc	0·01	33	1·5	5·9	3·43	13·6	5	0·37
Modal %	0·85	0·10	0·04	0·01			Av.F	0·36
							SD	0·09
							SE	0·02

SD, standard deviation; SE, standard error.
*Upper continental crust composition from Taylor & McLennan (1985) and McLennan *et al.* (2006).